Recent Advances in Integrated Die-Casting of Magnesium Alloys

Ye Tian¹, Yisheng Miao¹, Zhongyao Li¹, Shihao Wang¹, Qinghuai Hou¹, Junsheng Wang^{1,2,*}

- 1. School of Materials Science and Engineering, Beijing Institute of Technology, Beijing, 100081, China
 - 2. School of Multidisciplinary Science, Beijing Institute of Technology, Beijing, 100081, China
 - *Corresponding author. Tel.: +86 010 68915043. E-mail: junsheng.wang@bit.edu.cn (J.S. Wang)

Abstract: Prompted by the lightweighting strategy for new energy vehicles, integrated die-casting Mg alloy technology has emerged as a research hotspot due to its combined weight reduction potential and emission reduction benefits. This work focuses on four critical dimensions within the Mg alloy integrated die-casting technology system: material alloy design, forming defect mechanisms, multi-physics coupled numerical simulation, and component performance control strategies. It establishes a comprehensive material-process-performance analytical framework. This approach aims to overcome the fragmented nature of current theoretical research, providing foundational support for building a scientific theoretical framework for magnesium alloy integrated die-casting. Ultimately, it facilitates the continuous advancement of this technology towards higher precision and greater reliability.

Keywords: Integrated die-casting; Mg alloy; Defects; Numerical simulation

1 Introduction

Driven by China's "Dual Carbon" strategic goals (carbon peak and carbon neutrality) and *Energy-Saving and New Energy Vehicle Technology Roadmap 2.0*, the country's new energy vehicle (NEV) industry has achieved leapfrog development [1]. Meanwhile, vehicle lightweighting technology has emerged as the core strategic pathway for reducing energy consumption and carbon emissions, surpassing powertrain optimization and transmission efficiency improvements. Notably, Tesla's innovative application in the Model Y achieved a breakthrough 30% reduction in body weight, pioneering a global wave of automotive lightweighting innovation. From technical implementation perspective, modern automotive lightweighting engineering primarily relies on two innovative frameworks: material innovation and process innovation.

Within the lightweight material systems, Mg alloys offer distinct technical advantages due to their ultralow density of 1.7 g/cm³, 33% lighter than Al alloys and merely 23% of steel's density ^{[2]-[4]}. Research indicates that replacing 1 kg of traditional steel with Mg alloy enables a 30 kg CO₂-equivalent reduction over the vehicle's entire lifecycle. Currently, components such as steering wheels, shock towers, and instrument panel supports manufactured from Mg alloys have achieved

mass production and application, contributing significantly to carbon emission reduction. In summary, the exploration of Mg alloys holds significant potential for advancing effective and innovative lightweight solutions in the automotive industry [5].

Within the evolution of advanced manufacturing technologies, integrated die-casting represents revolutionary breakthrough compared to traditional forming processes such as stamping, welding, and forging. As illustrated in Fig. 1, this technology employs ultra-high-pressure die-casting machines coupled with high-precision mold systems to achieve 60-80% improvement in component integration, material utilization exceeding 95%, and 30%-50% reduction in manufacturing costs versus conventional processes [6]-[8]. Consequently, integrated die-casting has become a strategic enabler for cost reduction and efficiency enhancement in high-end manufacturing, extensive adoption in the automotive industry while expanding into aerospace and 3C product sectors. Industry implementations demonstrate its transformative impact: Tesla's proprietary die-casting system reduced the Model Y rear underbody assembly from 171 parts to just 2, cutting per-vehicle costs by 20% while enhancing structural integrity [9]; Volvo's Mega-Giga Casting enables die-casting technology of chassis components using an 8,000-tonne integrated casting machine [10]; while Toyota's Giga Casting 2.0 implementation halved vehicle assembly time, substantially boosting production efficiency [11].

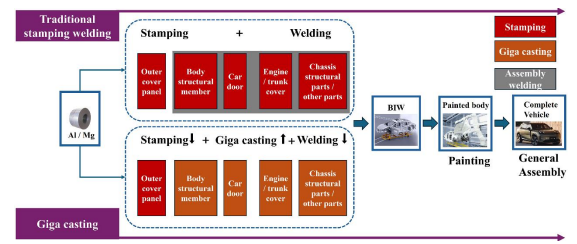


Fig.1 Comparison of Traditional Stamping-Welding and Giga Casting Integrated Manufacturing Processes

China's Mg alloy integrated die-casting technology system has entered a systematic development phase, achieving breakthrough progress in critical equipment R&D engineering applications. Leading manufacturers exemplified by Chongging Boao Magnesium-Aluminum Metal Manufacturing Co., Ltd. and Zhejiang Wanfeng Meridian New Material Technology Co., Ltd. have attained continuous, stable production of 1.6-meter-class automotive instrument panel support components. The National Engineering Research Center for Magnesium Alloys at Chongqing University, in collaboration with industrial partners, has successfully developed two critical structural components: rear floor assemblies and battery covers, utilizing 8,800-tonne ultra-large die-casting equipment. Engineering validation confirms these components achieve maximum projected areas on the order of 2.2 m², establishing an international size record for magnesium alloy automotive die-cast structures. Concurrently, Jilin University and FAW Foundry Co., Ltd. have collaboratively developed an Mg-Al-RE-Ca integrated die-casting Mg alloy, successfully implemented in the monolithic forming of battery packs for hybrid new energy vehicles [12],[13].

Current research on Mg alloy integrated die-casting faces significant technical barriers, with the core constraint being its rigid dependence on ultra-large, precision die-casting equipment. The limited accessibility of high-cost machinery (requiring clamping forces ≥4,000 T) restricts the number of global research institutions with comprehensive experimental capabilities. This directly impedes foundational data accumulation in the field, resulting in relatively scarce systematic research publications and reference-worthy engineering cases. Addressing this research landscape, this review focuses on four critical dimensions of the Mg alloy integrated die-casting framework: material alloy design,

forming defect mechanisms, multi-physics coupled numerical simulation, and component performance control strategies. Through systematic analysis of existing research achievements and technical bottlenecks, establish we comprehensive material-process-performance analytical framework. This work aims to overcome the fragmented nature of current theoretical studies, provide foundational support for building a scientific theoretical system for Mg alloy integrated die-casting, and ultimately advance this technology toward higher precision and greater reliability.

2 Alloy Composition Design for Integrated Die-Casting of Mg Alloys

Integrated die-cast magnesium alloy components present significant manufacturing challenges due to their ultra-large structural dimensions and complex geometries. Crucially, the prevalent adoption of thin-walled designs — with critical sections approaching ultra-thin dual configurations imposes constraints conventional heat treatment: steep thermal gradients induce macroscopic distortion compromising dimensional accuracy beyond design tolerances, while heterogeneous phase transformations promote residual microscopic stress accumulation that substantially elevates cracking susceptibility. Driven by these limitations, the industry prioritizes developing heat treatment-free alloy systems. Unlike traditional powertrain components requiring stringent mechanical properties, these emerging alloys focus on optimizing critical processing characteristics: enhanced melt fluidity, superior cast-filling capacity, improved deformation capability, and elevated-temperature creep resistance. Within this technical paradigm, conventional tensile strength requirements may be strategically relaxed, with balanced component performance achieved through synergistic optimization of casting process innovations and intrinsic material properties.

Among various Mg alloy systems, Mg-Al alloys have emerged as the preferred material for integrated die-cast components due to their superior casting characteristics: low melting point, reduced viscosity, and exceptional fluidity [14]-[16]. Based on compositional variations, Mg-Al systems are further classified into Mg-Al-Zn (AZ), Mg-Al-Mn (AM), Mg-Al-Si (AS), Mg-Al-RE (AE), Mg-Al-Ca (AX), and Mg-Al-Sr (AJ) series. Fig. 2 compares room-temperature mechanical performance across these die-cast Mg alloys. The

following sections systematically elaborate on research advances and application potential of each alloy system in integrated die-casting.

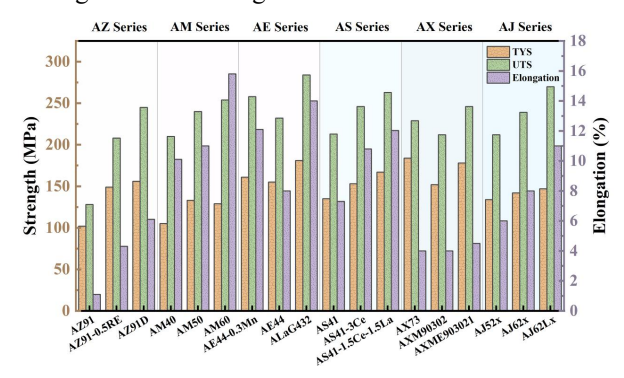


Fig.2 Mechanical properties of die-cast Mg alloys with different composition systems at room temperature [17-27].

2.1 Mg-Al-Zn alloys

In Mg-Al alloys, zinc (Zn) enhances melt fluidity due to its low melting point (~350 ° C). It has been demonstrated that 3 wt% Zn significantly improves fluidity, but exceeding this level can readily trigger hot cracking and porosity issues [28]. The castability and hot tearing susceptibility of AZ-series Mg alloys exhibit pronounced composition-dependent behavior: elevated Al content promotes microstructural embrittlement, while reduced Zn levels increase the propensity for microcrack formation [29]-[31]. As a primary alloying element, zinc effectively suppresses the formation of the Mg₁₇Al₁₂ phase in conventional AZ-series die-cast Mg alloys, thereby remarkably enhancing the creep resistance of Mg-Al-Zn alloys [32]-[35]. Beyond the Mg₁₇Al₁₂ phase, modulating the Al/Zn mass ratio enables the formation of diverse secondary phases within the alloy, including but not limited to τ-Mg₃₂(Al, Zn)₄₉, φ-Mg₅Zn₂Al₂, ε-MgZn, and the icosahedral i-Mg44Al15Zn41 phase [35]-[39]. To further enhance the performance of AZ alloys, minor elements are frequently introduced. The addition of Sn exceeding 0.3 wt.% improves castability and reduces die sticking, particularly in AZ91D, although excessive Sn additions impair fluidity [40]. Incorporating 0.5 wt.% Sr into AZ91 alloy lowers the liquidus temperature and increases fluidity by 14%. Notably, the combined addition of Sr and B produces a synergistic effect, resulting in a remarkable increase in fluidity of up to 157% [41]. Yim et al. demonstrated that the fluidity of AZ31 alloy melt increases with Ca additions (up to 0.5 wt.%), attributable to Ca's grain refining effect [42]. Regarding age-hardening behavior, Srinivasan et al. observed that Pb additions prolong the time required for AZ91 alloy to reach peak hardness [43]. Conversely, minor Nd additions, while retarding the aging kinetics in AZ80 alloy, ultimately enhance its mechanical properties ^[44]. Controlled additions of rare earth (RE) elements, such as by optimizing the La/Nd mass ratio, can improve fluidity and hot tearing resistance ^[45]. It should be noted, however, that excessive RE content impairs both corrosion resistance and ambient-temperature strength ^{[46]–[48]}.

2.2 Mg-Al-Mn alloys

Mg-Al-Mn and Mg-Al-Zn-Mn alloys currently dominate over 90% of structural applications [49]. However, the prevalent AZ91 alloy (Mg-9.5Al-0.5Zn-0.3Mn, wt.%) exhibits insufficient toughness (elongation <10%) for energy-absorbing components such as seat frames. In contrast, AM60 (Mg-6Al-0.3Mn) and AM50 (Mg-5Al-0.3Mn) alloys are preferred for automotive lightweighting due to superior castability, ductility, and corrosion resistance. High-pressure die-casting (HPDC) produces characteristic "sandwich" microstructure under rapid cooling: a fine-grained dense surface layer and a coarse-grained porous core region [50],[51]. While Weiler et al. [52] attributed the skin/core hardness discrepancy in AM60 to grain size effects, Biswas et al. [53] demonstrated that the area fraction of β-Mg₁₇Al₁₂ phase plays a more dominant role. Digital Image Correlation (DIC) analysis by Zhang et al. revealed strain localization predominantly in pore-rich zones, with β-phase distribution having minimal impact on deformation heterogeneity, as shown in Fig. 3 [54]. Furthermore, Sn addition refines eutectic phase boundaries and progressively enhances hardness [55]. In Mg-6Al-0.5Mn-2Ca alloys, Al₂Ca phase co-precipitation with creep-induced fine particles effectively suppresses dislocation climb/glide mechanisms [56].

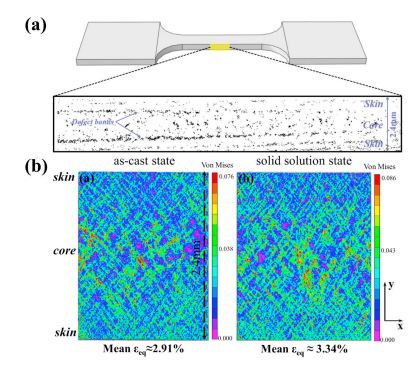


Fig.3 (a) Representative binary image depicting through-thickness distribution of the porosity in the plate. The areas in black are porosity, and the areas in white are material, (b) Contour plots of the equivalent strain εeq after 3% macroscopic axial deformation under tension for a selected region of AM60 alloy under as-cast state and solid solution state [54].

2.3 Mg-Al-RE alloys

The strengthening effect of rare earth (RE) elements on Mg alloys was first documented as early as the 1930s. Research by Foerster (1972-73) demonstrated that adding 1% RE substantially enhanced the creep resistance of Mg-Al-based alloys. Notably, at lower Al levels, RE elements improved the creep strength of Mg-Al alloys more effectively than Si additions [57]. The AE42 alloy established benchmark (Mg-4Al-2RE), as creep-resistant die-cast magnesium alloy, outperforms AZ91 at 423 K (150°C) but suffers from hot tearing during casting and rapid creep degradation above 150°C [58]-[60]. This accelerated the development of AE44 (Mg-4Al-4RE), which exhibits superior fluidity, an optimal strength-ductility balance, and a higher eutectic volume fraction [61],[62]. Consequently, AE44 has become the material of choice for automotive mega-castings such as engine mounts and the 2016 Ford Focus subframe [63]. Notably, industrial RE additions utilize mixed rare earths (typical: 60% Ce, 30% La, \leq 10% Nd, trace Pr) derived from direct ore conversion without elemental separation. Recent cost reductions for single-element (La/Ce) and binary (Ce + La) RE mixtures relative to quaternary blends have spurred development of novel AE alloys [64]. Zhang et al. fabricated Mg-4Al-xRE-0.3Mn (RE=La or Ce, x=1, 2, 4, 6 wt.%) via high-pressure die casting. The Mg-4Al-4La-0.3Mn and Mg-4Al-4Ce-0.3Mn alloys demonstrated exceptional tensile properties and thermal resistance below 200°C, attributed to thermally stable Al11RE3 strengthening phases with high volume fractions [65],[66]

2.4 Mg-Al-Si alloys

The Mg-2Al-1Si (AS21) alloy represents a specialized creep-resistant die-casting material developed for automotive engine applications [67]. Blum et al. [68] established that Mg₂Si particles distributed along grain boundaries significantly enhance long-term creep performance, enabling superior resistance compared to conventional AZ91 and Mg₁₇A1₁₂-containing alloys under low strain rates and elevated temperatures. However, coarse Mg₂Si phases exert detrimental effects, necessitating precise morphological control as a critical pathway for developing high-performance Mg-Al-Si alloys. Strategic elemental additions effectively refine Mg₂Si: Sr additions progressively regularize particle morphology [69]; Sb forms high-melting Mg₃Sb₂ phases that serve as heterogeneous nucleation sites for refined Mg₂Si ^[70]; while Ce simultaneously transforms acicular Mg_2Si into fine fibrous structures and generates growth-inhibiting $CeMg_2Si_2$ phases, both contributing to mechanical property enhancements surpassing those achievable with Mg_2Si alone [71],[72].

2.5 Mg-Al-Ca alloys

Ca emerges as the most promising alloying element for magnesium alloys due to its cost efficiency coupled with multifunctional benefits: enhanced creep resistance, improved castability, and reduced flammability [46],[73],[74]. These advantages have enabled commercial Mg-Al-Ca alloys such as the MRI series (Mg-Al-Ca-Sr/Sn-Sr) and AXJ530 (Mg-5Al-3Ca-0.2Sr) [64]. Research indicates that increasing Ca content significantly reduces hot tearing susceptibility in Mg-Al-Ca alloys, with minimal influence from Al variations [75]. Under high-stress creep conditions, AZ91 outperforms MRI153 due to superior work-hardening capacity and yield strength [76]. Zhang et al. [26] developed novel AX die-casting alloys employing precisely controlled trace Ca additions to achieve stable solid solution strengthening, thermally concurrently enhancing room- and elevated-temperature strength, distinct from the eutectic phase modification strategy in MRI alloys. Through EET theory calculations, Min et al. revealed that Ca dissolution in the Mg₁₇Al₁₂ phase increases bonding strength, homogenizes covalent electron distribution, and elevates phase melting point, thereby improving overall alloy performance [77].

2.6 Mg-Al-Sr alloys

Mg-Al-Sr alloys were developed to replace rare earth elements with alkaline earth additions [78],[79]. The first-generation Mg-5Al-2Sr (AJ52x), when processed with optimized parameters, exhibits superior creep elevated-temperature performance, resistance. castability. This is attributed to reduced aluminum supersaturation in primary magnesium and the formation of high-melting-point Al-rich Zr phase, replacing Mg₁₇Al₁₂ phase [80]-[82]. The enhanced Mg-6Al-2Sr (AJ62x) system delivers: (i) die-cast versions with exceptional creep resistance, hot tearing resistance, and corrosion resistance; (ii) high-ductility variants (AJ62Lx) that improve tensile strength and elongation at room temperature by precisely tuning aluminum solid solubility while maintaining castability [83].

3 Typical Mg alloy die casting defects

Large-scale integrated magnesium die castings are prone to various defects—including porosity, shrinkage porosity, hot tearing, cold shuts, and distortion (Fig. 4)—

due to their thin walls, complex geometries, non-uniform temperature distribution, and gas entrapment during high-speed melt filling. These defects significantly compromise component performance and pose limitations on broader industrial implementation of magnesium integrated die casting. Unlike gravity casting, defect formation mechanisms in magnesium die casting involve greater complexity. This section provides an overview of the characteristics and contributing factors for the typical defects illustrated in Fig. 4.

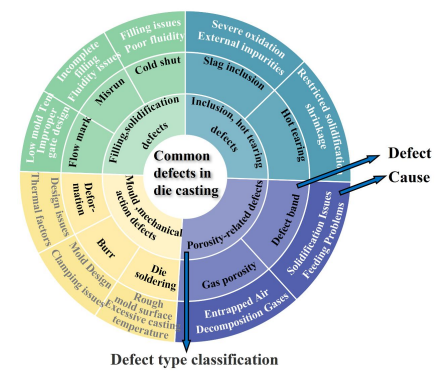


Fig.4 Common defects in die casting

3.1 Porosity-related defects

The primary drawback of HPDC is porosity. Depending on pore location and size, castings exhibit position- and direction-dependent properties in ductility, strength, and corrosion resistance. Early research confirms that extrinsic pore defects become the dominant limiting factor for ductility when pore volume fraction exceeds a critical threshold [50],[84]. Extensive studies have established correlations between porosity levels and ductility/fracture behavior in Mg castings. For instance, Chadha et al. [84] and Jung [85] modified the classical Brown-Embury model by incorporating crack tip radius and size parameters to predict tensile ductility [86]. Based morphological characteristics and formation mechanisms, porosity defects are categorized into gas porosity and defect bands.

3.1.1 Gas porosity

Gas porosity primarily forms through air entrapment during mold filling and decomposition of gaseous compounds. The high-speed injection characteristic of die casting promotes turbulent flow, making entrapped gas porosity predominant. Such defects cannot be fully eliminated even with vacuum-assisted systems. Typically exhibiting smooth, spherical/elliptical morphologies with equivalent diameters of 20-100 µm, these pores demonstrate random distribution patterns affected by

component thickness or dimensions [87],[88].

Porosity defects are characterized by destructive methods and non-destructive techniques, complemented by microscopy and density measurement [89],[90]. As shown in Fig. 5, Wu et al. [91] characterized the morphology and distribution of typical gas pores in die-cast samples using X-ray tomography, performing 3D void reconstruction with VGStudio Max 2.0 software. This analysis demonstrates that gas pores persist despite vacuum-assisted die casting. Furthermore, morphological parameters - including roundness, sphericity, and shape factors—enable precise classification of void defects into distinct categories: gas pores, gas-shrinkage pores, net-shrinkage, and isolated shrinkage [92],[93]. Miao et al. [88] systematically quantified the influence of micropore size/morphology/distribution on mechanical properties across wheel hub sections using X-ray CT.

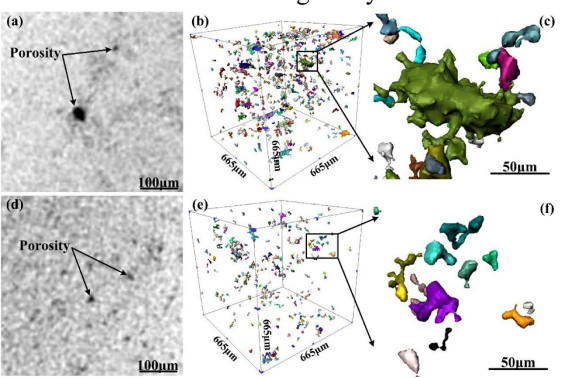


Fig.5 Typical morphology and distribution of porosities in the microstructure of (a-c) sample A and (d-f) sample B. (a) and (d) 2D slice images scanned by X-ray tomography, while (b,c) and (e-,f) 3D images reconstructed by VGStudio Max 2.0 software [91].

3.1.2 Defect band

Defect bands — void-aggregated ribbon-like structures in HPDC Mg alloys—form through synergistic effects of melt flow, solidification behavior, and processing parameters [94],[95]. As shown in Fig. 6, they manifest as single, double, or multiple bands with either contour-aligned or irregular distributions, correlating strongly with externally solidified crystals (ESCs) [95]. Wu et al. [96] identified three distinct microstructural zones: 1) Surface-to-band interface: Minimal voids with fragmented, non-clustered ESCs yielding dense structure; 2) Defect band: High-density irregular voids concentrated at grain boundaries of fine ESCs; 3) Core region: Coarse clustered ESCs promoting randomly distributed shrinkage porosity along grain boundaries.

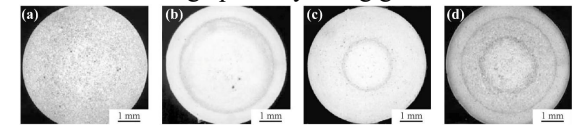


Fig.6 Defects bands with different morphology and distribution characteristics at cross section of Mg alloys die casting samples.(a) AZ91; (b) AM20; (c) AM60; (d) AM50 [95].

3.1.3 Factors affecting porosity-related defects

Processing stands as the primary factor governing porosity-related defects. Conventional HPDC inherently yields elevated gas content, failing to meet the demands of high-strength/high-ductility components. Although vacuum-assisted die casting (VADC) significantly reduces component gas content, residual levels remain at 10-15 cc/100g [97],[98]. Super-vacuum die casting (SVDC) achieves <3 cc/100g for heat-treatability, but requires substantial capital investment. Pore-free die casting (PFDC) technology demonstrates superior gas reduction by injecting reactive oxygen into dies and shot sleeves to displace air, triggering self-evacuation via oxygen-melt reactions, as shown in Fig. 7 [99]. Notably, PFDC applications remain predominantly Al-based; its technical compatibility with Mg alloys, challenged by elevated chemical reactivity, warrants further investigation.

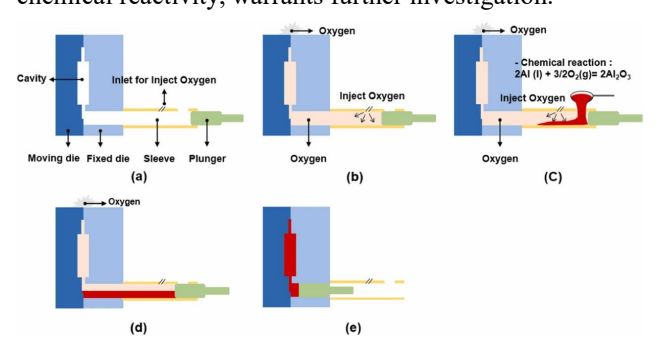


Fig.7 Schematic diagrams of the PFDC process [99].

Process parameters constitute the primary control factor for porosity defects in Mg alloy die castings. Optimizing injection speed provides a cost-effective alternative expensive, low-efficiency technology by refining grain structure. Research confirms that high-speed injection enhances melt turbulence and tensile stress, fragmenting ESCs dendrites to reduce their population while improving feeding capacity during solidification to minimize porosity [22],[100]-[102]. However, excessively high speeds diminish ESCs content, triggering defect band migration toward the core with reduced width and intensified porosity clustering. Accelerating low-speed phases or shortening pouring delays amplifies this effect. Increased high-shot speeds disperse ESCs and sustain band migration, whereas absence of high-speed injection induces bifurcated defect bands [96].

Mold and gating system design critically influence porosity defects in die castings. Li et al. [103] engineered a specialized gating system that subjects melt to high shear stress within runners, effectively fragmenting coarse ESC dendrites and enhancing feeding capacity. This approach

yielded a homogeneous AZ91 magnesium microstructure with reduced ESCs population and minimized porosity, substantially improving mechanical properties.

3.2 Inclusion and hot tearing defects

In HPDC, inclusions and hot tearing constitute critical defects.

3.2.1 Inclusion defects

Inclusions primarily originate from oxidation during melting, flux residues, and external contamination. When exposed to air without protective coverage, molten Mg alloys undergo intense oxidation forming MgO inclusions as shown in Fig. 8(a). These brittle phases act as stress concentrators that initiate microcracks. While gravity casting employs protective gas purging or sulfur powder application in molds to prevent combustion, both methods are incompatible with HPDC, exacerbating oxide and dross formation [104]. Beyond endogenous oxides, exogenous non-metallic inclusions arise from die lubricant residues or tooling wear particles. Notably, advancements in melt purification have substantially reduced flux/contaminant-derived inclusions, rendering oxides the predominant contributor in modern casting systems [105].

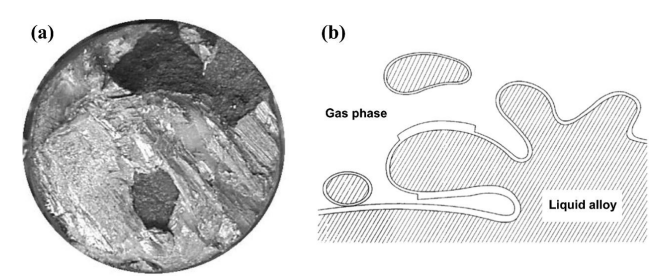


Fig.8 (a) Fracture surface of a pure Mg test bar cut from a top-filled cast plate showing dark features subsequently identified as oxide films, (b) Sketch of a surface-film entrainment event in a light alloy casting [106],[107].

Cashion et al. [108],[109] identified monolayer MgO-MgF2surface films via XPS/AES analysis. However, oxide films exhibit multilayered configurations: mold-filling turbulence induces film folding, forming double-layer entrainment defects (bifilms) when dry surfaces overlap, as shown in Fig. 8(b) [107]. Pettersen et al. [110] reported a trilayer evolution, where initial MgO transforms into MgF2/MgO-rich/ MgF2 sandwich structures through F diffusion. Peng et al. [111] demonstrated that bifilms in AZ91 melt filter and capture Al₈Mn₅ particles, subsequently dragging intermetallics to form ultra-large aggregates that exacerbate detrimental effects. Consequently, the "Bifilm Index" was established to quantify casting quality by measuring the total length

of entrained double oxide films on polished surfaces of standardized reduced-pressure test samples [112].

3.2.2 Hot tearing

Hot tearing, a critical defect in HPDC processes, significantly impacts casting quality. It is fundamentally distinguished from cold cracking by its formation above the solidus temperature, initiated when localized stresses exceed the strength of partially solidified metal coupled with inadequate feeding [113],[114]. Large structural castings exhibit greater susceptibility than smaller components. The hot tearing susceptibility (HTS) quantifies this propensity as shown in Fig. 9 [115]. Moreover, Song et al. [30] have comprehensively analyzed key influencing factors and susceptibility laws governing Mg alloy hot tearing behavior. Thus, this section provides a concise overview.

3.2.3 Factors of inclusions and hot tearing

The production of high-quality lightweight alloy castings is critically dependent on melt treatment efficiency. Mg alloys exhibit high reactivity with gases such as O₂, water vapor, and N₂ at elevated temperatures, leading to inclusion formation in the melt that compromises casting integrity and mechanical properties. Consequently, melt treatment techniques fundamentally govern inclusion content. Significant global advancements have been achieved in Mg alloy melt purification technology, which is categorized into flux-based and flux-free methods according to flux usage.

Flux refining, a standard process for magnesium melt purification, promotes inclusion wettability through flux-melt interactions, inducing agglomeration into larger particles. These particles separate from the melt via gravitational settling to the crucible bottom [116]. While halide salt mixtures e.g., MgCl₂, KCl, and CaCl₂ are predominantly employed, this method faces industrial limitations due to environmental concerns, flux-derived inclusions, and metal loss.

Flux-free methods, as innovative systems for Mg alloy melt purification, remove inclusions via physical mechanisms while eliminating secondary contamination risks inherent to flux-based approaches and mainly include electromagnetic purification, ultrasonic purification, bubble flotation, and filtration purification.

Electromagnetic purification leverages the conductivity differences between metals and non-metals to achieve dynamic separation of inclusions under a magnetic field. This method is particularly effective for removing fine solid-liquid inclusions with particle sizes

at the micron scale and densities similar to molten Mg. However, the efficiency degradation caused by slag accumulation on container walls must be addressed [116],[117]. Ultrasonic purification is primarily employed to remove oxide inclusions. It utilizes ultrasonic phenomena to accelerate the collision-coalescence process of oxide inclusions within a standing wave field [118]. This method offers environmental benefits while simultaneously facilitating grain refinement [119]-[122]. Nevertheless, its industrial-scale implementation is constrained by the limitations of high-power ultrasonic generator systems [116]. Bubble flotation technology removes inclusions through the dual mechanisms of adsorption and flotation by inert gas microbubbles. It offers simple operation and environmental friendliness. However, optimization of process parameters, such as bubble size and flow rate control, remains essential for enhancing process efficiency [116]. Filtration purification, serving as a final refining step, employs multistage filter media to intercept inclusions, thereby significantly enhancing melt cleanliness. However, this method is inherently limited by filter clogging and high maintenance costs [123],[124].

Current research prioritizes coupling and optimizing multiple technologies, such as electromagnetic-ultrasonic refining and integrated bubble flotation-filtration. Simultaneously, intelligent equipment development, like self-cleaning filters and adaptive control systems, is emerging as key to overcoming technical bottlenecks. Despite industrial adoption challenges (e.g., high investment, narrow process window), non-flux refining remains crucial for advancing high-quality Mg alloy casting due to its sustainability and precision control capabilities.

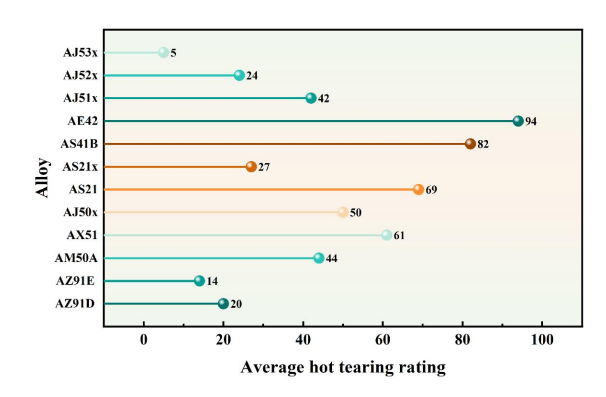


Fig.9 Average hot tearing rate of Mg alloys [115].

3.3 Filling and solidification defects

During die casting, molten metal is prone to defects during high-velocity filling and rapid solidification, directly compromising the casting's mechanical properties, air-tightness, and surface quality. These defects primarily fall into three categories: cold shut, misrun, and flow mark.

3.3.1 Cold shut

Cold shuts are linear defects formed at converging melt fronts due to insufficient thermodynamic conditions during die casting (Fig. 10(a)), essentially representing discontinuous interfaces caused by inadequate kinetic energy at flow fronts [125]. Particularly prevalent in complex thin-wall castings, Pareto analysis identifies them as the primary improvement target of defect-related issues [126]. When the melt temperature falls below the liquidus or the mold temperature is insufficient, premature solidification of flow fronts occurs, where oxide layers impede fusion [127]. What's more, inadequate injection pressure or velocity undermines the penetration capacity of molten metal flow, while faulty gating system design (e.g., undersized runner cross-sections, excessive branch runner length variations) causes temporal asynchrony in multiple flow fronts, exacerbating cold shut risks [127]. Industrial case studies confirm that elevating mold temperature, injection velocity, and optimizing gate locations significantly reduce cold shut occurrence [128]. Numerical simulations further reveal that melt convergence angles >90° drastically increase risk, necessitating runner topology optimization to maintain angles within 30°~60° [129].



Fig. 10 (a) Cold shut, (b) Misrun, (c) Flow marks

3.3.2 Misrun

As illustrated in Fig. 10(b), misruns manifest as localized casting deficiencies due to incomplete cavity filling, primarily attributable to three factors: melt fluidity, filling dynamics, and mold thermal equilibrium [130]. Inadequate fluidity often stems from improper alloy composition or insufficient superheat temperature, while deficient injection pressure and shortened dwell time compromise filling dynamics, preventing the melt from overcoming cavity flow resistance. Undercooled zones caused by mold design defects accelerate solidification at flow fronts, disrupting filling continuity. [131]–[134]. Notably, machine learning (ML)-based process parameter optimization is emerging as a novel approach to address misruns in complex castings [135]–[137].

3.3.3 Flow marks

As shown in Fig. 10(c), flow marks manifest as wavy/streaky surface defects formed by temperature fluctuations or delayed solidification at melt flow fronts, with morphology directly correlating to flow stability [138]. Excessive mold surface roughness or uneven release agent spraying increases contact resistance between flow fronts and mold walls, inducing periodic velocity variations that generate visible marks. Uncontrolled temperature gradients in molten metal cause localized front solidification, triggering stick-slip flow patterns that exacerbate defects. Research demonstrates that mold surface polishing, precision temperature control systems, and pulsed release agent spraying effectively mitigate flow marks [139].

3.4 Mould and mechanical action defects

3.4.1 Die soldering

The flow behavior of molten metal during casting is significantly governed by key parameters, including plunger speed, mold temperature, shot sleeve temperature, and melt pressure [140],[141]. Unlike the misruns discussed in Section 3.3, which can be avoided through parameter adjustment, sticking defects resist elimination via free parameter modulation, particularly in Al alloys. The mechanism underlying involves: formation intermetallic phases at Al-Fe interfaces, where micro-scale Al-rich liquid phases precipitated between phases act as adhesive "welding" casting to mold [142],[143]. Alex et al. [144] proposed a novel theory: intermetallic phases essentially represent thermomechanical wear manifestations, as traditional thermodynamic/kinetic theories fail to fully explain sticking in HPDC, a perspective endorsed by Terek et al. [145].

In contrast, Mg alloys exhibit markedly lower sticking tendency in HPDC due to low Mg-Fe affinity [146]. Sticking in Mg alloys primarily correlates with Al/Mn content and Al-Fe-Mn intermetallic phase formation [146]. Benefiting from reduced sticking risks, Mg alloy die casting offers an expanded process window, enabling mass production of large automotive components with wall thicknesses <2mm.

3.4.2 Burrs

Burrs formation (also termed flash or fins) in integrated die castings fundamentally results from molten metal penetration into mold parting lines or moving component gaps under high pressure. Contributing factors include: loss of fit precision due to mold aging, improper machine parameter settings, and flawed

gating/venting system design. Notably, new molds may initially produce defect-free castings; however, with increasing cycles, release agent residue accumulation and moving part wear trigger progressive flash deterioration, evolving from micro-burrs to macro-fins. Table 1 comprehensively categorizes Burrs causes and corresponding removal methods [147].

Table 1 Causes and corresponding removal methods of burrs [147]

	Burr Formation Causes	Removal
		Methods
Mold-Related Factors	Mold wear/aging	
	Insufficient mold	
	manufacturing precision	
	Mold deformation	
	Parting surface damage	Manual or mechanical
	Excessive clearance/wear	
	of movable components	removal
D.	Insufficient clamping	Trimming
	force	Grinding
	Excessive injection	Shot blasting
	pressure	Thermal
Process	•	explosion
Parameter	Overhigh injection speed	method
Factors	Excessively high melt	Chemical dissolution
	temperature	
	Non-uniform/overh	High-pressure
	igh mold temperature	water jet
	Malfunction of clamping	Ultrasonic
Equipment	mechanism	removal
Factors	Poor parallelism of die	
	casting machine	
Material	High fluidity of molten	-
Factors	metal	

For integrated die casting of large, complex thin-walled components, burrs control carries critical significance: it not only compromises aesthetics and dimensional accuracy, but its removal constitutes labor-intensive post-processing that substantially elevates costs. With advances in artificial intelligence, robot-assisted flash removal is emerging as an efficiency-enhancing solution [148],[149].

3.4.3 Deformation

Deformation constitutes a critical defect in large-scale die castings, manifesting as post-cooling/ejection deformations including bending, twisting, and localized collapse, fundamentally attributed

to non-uniform residual stresses exceeding material stiffness limits [150]. Root causes encompass four dimensions: primarily heterogeneous shrinkage induced by differential thermal expansion coefficients between casting and mold; secondly, localized overcompaction or underfilling triggered by inadequate material fluidity; thirdly disruption of melt overflow-solidification synchronization due to improper injection speed/temperature; and finally design-phase deficiencies involving excessive tolerance buffers, inaccurate shrinkage allowance calculations, and insufficient process capability. Particularly for components with significant wall thickness variations, non-uniform cooling prevents precise simulation of quenching resulting in compromised dimensional tolerance compliance that necessitates systematic deviation pattern analysis by process engineers.

Multi-pronged strategies are implemented for deformation control: adopting heat-treatment-free materials to eliminate quenching deformation; optimizing product geometry to ensure wall thickness uniformity and suppress shrinkage gradients; redesigning gates to enhance melt flowability while improving venting to prevent gas-induced distortion; precisely regulating injection speed, temperature, and intensification pressure to achieve uniform filling and residual minimization; utilizing CAE simulation to predict risks and optimize structural design; and ultimately employing calibration dies with automatic shaping functions for dimensional rectification [151],[152].

4 Numerical simulation

Numerical simulation technologies have dramatically accelerated material development, with breakthroughs in high-throughput computing over the past two decades establishing multi-scale modeling as a cornerstone tool in materials R&D [153]-[155]. Before simulation adoption, foundry process evaluation relied on resource-intensive trial production methods with low efficiency [156]. Since the inaugural numerical simulation of casting solidification in 1962, this technology has become indispensable for process optimization, its accuracy now widely endorsed by industry [157]. Particularly given increasingly complex casting geometries and rising costs, numerical simulation has emerged as a pivotal tool for foundry process enhancement. As summarized in Table 2, Mg alloy die casting simulations span full-scale chains from macro thermo-fluid dynamics to microstructural evolution. This section systematically elucidates the principles and applications in Mg alloy die casting, while analyzing current challenges and future trajectories.

Table 2 Numerical simulation scale and method of die casting Mg alloy [158,159]

	andy		
Scale	Simulation	Common	Representati
Level	Objectives	Methods	ve Tools
Macroscal e	Melt filling behavior, temperature/stre ss fields	Finite Element Method	FLOW-3D, ProCAST, MAGMASof t
Mesoscopi c scale	Dendrite growth, defect formation	Phase Field, Cellular Automata	MICRESS
Microscal e	Grain nucleation/grow th	Cellular Automata, Monte Carlo	DICTRA, DAMASK
Atomic Scale	Interfacial energy diffusion kinetics	Molecular Dynamics, First-Principl es Calculations	LAMMPS, VASP

4.1 Macro-scale simulation of die-casting Mg alloy

Macroscopic simulation of Mg alloy casting primarily focuses on modeling molten metal flow behavior patterns, thermal fields, and stress distributions. With revolutionary advances in numerical simulation technologies, such macro-scale process simulations have now matured and gained extensive industrial implementation.

4.1.1 Flow field simulation

The mold filling process in casting fundamentally adheres to three physical conservation laws: mass, momentum, and energy. This process is fully described by a set of governing equations comprising: the continuity equation, Navier-Stokes equations, Volume of Fluid (VOF) equation, and energy equation:

1) Continuity equation-mass conservation equation

The continuity equation is the basic description of the mass conservation law of moving fluid [160]:

$$\frac{\partial \rho}{\partial t} + \nabla(\rho V) = 0 \tag{1}$$

Where ρ is the density of molten metal, V is the velocity of the fluid, t is time,

For incompressible fluids, the density is independent of time and location. Whether in steady state or unsteady state, the continuity equation can be

simplified as:

$$\frac{\partial u}{\partial x} + \frac{\partial v}{\partial y} + \frac{\partial w}{\partial z} = 0 \tag{2}$$

Where u, v, w are the velocity components along the x, y, z directions, respectively.

2) Navier-Stokes equation-momentum conservation equation [161]:

$$\rho \frac{DV}{Dt} = -\nabla P - D\tau + \rho G \tag{3}$$

where G is gravity, τ is the stress tensor, D is the partial differential operator.

For incompressible fluids:

$$\nabla \tau = -\mu \nabla^2 V \tag{4}$$

Where μ is the dynamic viscosity, Then the Navier-Stokes equation can be rewritten as:

$$\rho \frac{DV}{Dt} = -\nabla P + \mu \nabla^2 V + \rho G \tag{5}$$

3) Energy conservation equation

According to the Fourier heat conduction law and the law of conservation of energy, the energy conservation equation of heat transfer in molten metal can be obtained [159]:

$$\frac{\partial(\rho c_p T)}{\partial t} + \frac{\partial(\rho c_p T u)}{\partial x} + \frac{\partial(\rho c_p T v)}{\partial y} + \frac{\partial(\rho c_p T w)}{\partial z} \\
= \frac{\partial}{\partial x} \left(\lambda \frac{\partial T}{\partial x}\right) + \frac{\partial}{\partial y} \left(\lambda \frac{\partial T}{\partial y}\right) + \frac{\partial}{\partial z} \left(\lambda \frac{\partial T}{\partial z}\right)$$
(6)

where T is the temperature of the molten metal, C_p is the equal pressure specific heat capacity, λ is the thermal conductivity of the molten metal. When the density, isobaric specific heat capacity, and thermal conductivity are constant, the above formula can be changed to:

$$\frac{\partial T}{\partial t} + u \frac{\partial T}{\partial x} + v \frac{\partial T}{\partial y} + w \frac{\partial T}{\partial z} = \alpha \left(\frac{\partial^2 T}{\partial x^2} + \frac{\partial^2 T}{\partial y^2} + \frac{\partial^2 T}{\partial z^2} \right) \tag{7}$$

where $\alpha = \frac{\alpha}{\rho c_n}$ is the diffusion coefficient of molten metal,

4) Volume function equation:

For incompressible fluids [162]:

$$\frac{\partial F}{\partial t} + u \frac{\partial F}{\partial x} + v \frac{\partial F}{\partial y} + w \frac{\partial F}{\partial z} = 0$$
 (8)

Most fluid flow simulations operate under low Mach number conditions (Ma<0.3), where fluid compressibility is negligible, permitting incompressible flow treatment. Using compressible solvers for such scenarios necessitates prohibitively small time steps, drastically increasing computational costs-a fundamental driver for developing dedicated incompressible solvers. The core challenge incompressible computation lies in the continuity equation manifesting as a divergence-free constraint $(\nabla \cdot u=0)$ rather than a time-evolution form, requiring pressure (lacking a time-dependent term) to satisfy this constraint [163].

Marlow's Marker-and-Cell (MAC) method solves pressure by deriving a Poisson equation from the divergence of the momentum and continuity equations [164]. Amsden's Simplified MAC (SMAC) employs a predictor-corrector approach: velocities are predicted and then corrected via solving a Poisson equation for a scalar potential [165]. In contrast, Chorin's Artificial Compressibility Method (ACM) eliminates the need for solving a Poisson equation, but is limited to obtaining steady-state solutions [166].

4.1.2 Temperature field simulation

Numerical simulation of the temperature field in casting typically involves two distinct phases: filling and solidification. The filling stage constitutes a transient convection-diffusion problem.

$$\frac{\partial}{\partial t}(\rho cT) + \nabla(\rho cUT) = \nabla(\lambda \nabla T) + S_T \tag{9}$$

where C is the specific heat capacity, S_T is the heat source term. The transient temperature field during solidification can be obtained by solving the Fourier heat conduction equation. The solution requires initial conditions and boundary conditions, with the latter typically being the third kind (Robin condition), representing heat exchange at the boundary, expressed as:

$$-\lambda \frac{\partial T}{\partial n} = h(T - T_{\infty}) \tag{10}$$

Where T and T_{∞} are the temperatures at the interface contact between the casting and the mold, respectively, h is the interface heat transfer coefficient between the

casting and the mold.

The calculation of the temperature field in casting must account for the latent heat release during the liquid-solid phase transition. Incorporating latent heat, the unsteady heat conduction equation becomes:

$$\rho\left(c_p - L\frac{\partial f_s}{\partial T}\right)\frac{\partial T}{\partial t} = \lambda\left(\frac{\partial^2 T}{\partial x^2} + \frac{\partial^2 T}{\partial y^2} + \frac{\partial^2 T}{\partial z^2}\right) \tag{11}$$

where L is the latent heat of solidification of the alloy, f_s is the solid fraction.

As analyzed in Section 3, temperature field distribution critically influences casting defect formation. Therefore, computer simulation-based process optimization before physical casting experiments can effectively prevent such defects. The temperature gradient criterion (G), originally proposed by Bishop and Pellini, was refined by the Niyama group in 1982. They established a strong correlation between the critical temperature gradient required for sound castings and solidification time, reformulating it as $G/(R_c)^{1/2}$, known as the Niyama criterion [167]. Its validity has recently been verified for TiAl [168], Al [169], and Mg [170] alloys.

4.1.3 Stress field simulation

During solidification, castings evolve through liquid, mushy, and solid states, developing internal stresses from three sources: (1) thermal stresses due to uneven wall thickness and cooling rates; (2) phase transformation stresses from liquid-solid and subsequent solid-state phase changes; (3) mechanical constraints from mold/core resistance to shrinkage. Given the complexity of stress-strain relationships, current research focuses predominantly on the mushy and solid zones (particularly post-solidification regions), whereas the liquid zone remains less explored.

For thermal stress calculation in the solid region of castings, the thermo-elastoplastic model is most widely employed. It neglects viscous effects: materials deform elastically before yielding and plastically post-yielding, with both elastic modulus and yield stress being temperature-dependent. Crucially, these parameters approach zero as temperature nears the melting point. The constitutive relationship is governed by:

$$\{d\sigma\} = [D]_{ep}\{\{d\varepsilon\} - \{d\varepsilon_T\}\}$$
(12)

where $\{d\sigma\}$ is the stress increment, $[D]_{ep}$ is the elastoplastic matrix, $\{d\epsilon\}$ and $\{d\epsilon_T\}$ is the total strain increment and thermal strain increment.

4.2 Mesoscale simulation of die-casting Mg alloy

Conventional casting relies on empirical process design for quality control, lacking quantitative characterization of temperature/stress fields during forming and observation of melt flow-solidification behavior with defect evolution. In contrast, full-process numerical simulation significantly enhances R&D fault tolerance: it enables a transition from heuristic trial-and-error to scientific modeling, visualizes dynamic multi-physics responses, and accurately predicts defect types, distribution, and dimensions, thereby optimizing processes, improving product quality and productivity, while reducing manufacturing costs.

Porosity defects critically restrict the heat treatability of castings and substantially degrade product quality. As a key initiator of fracture susceptibility, this issue has garnered significant attention from researchers and manufacturers. As shown in Fig. 10 (a1-f2), utilizing Magma simulation software, Cao et al. [171] demonstrated that while gas vortices in conventional die casting impede venting efficiency, unidirectional upward gas movement in vacuum die casting drastically reduces localized gas entrapment constrained by flow fields. This mechanism minimizes gas capture by molten metal, enabling effective porosity control. Li et al. successfully predicted pore distribution in WE54 alloy via ProCAST [170]. Wang et al.'s [172] numerical simulations of Hot Tearing Index (HTI) for Mg-Y and Mg-Zn-Y alloys revealed close alignment between predicted crack locations/severity and experimental results in Mg-Zn-Y alloys (Fig. 10 (g-j)). However, two critical limitations of the HTI module must be noted: First, simulation validity depends on comprehensive stress-strain hardening data accurate composition and mold temperature sensitivity complete mechanical analysis requires databases. Second, HTI values are non-comparable across alloy systems; the module is solely applicable to well-characterized alloys with systematically established parameters.

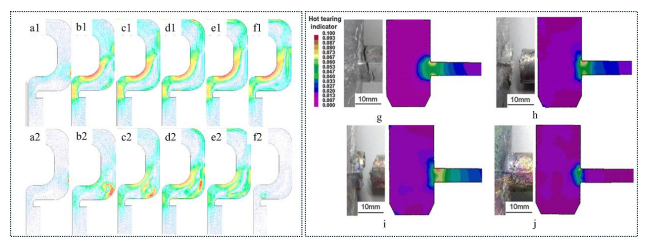


Fig. 10 The velocity vector of vacuum die casting filling (a1-f1); the velocity vector of ordinary die casting filling (a2-f2) [171]; comparison between the simulation results of HTI and experimental observations for Mg-4.5Zn-xY alloys at the mould temperature of 250°C, (g) x=0, (h) x=0.4, (i) x=0.9, and (j) x=2 [172].

Defect formation exhibits significant correlations

with mold design and process parameters; optimizing these factors effectively mitigates defects. Amol et al. [173] optimized cooling channel configurations using ANSYS and adjusted gate thickness based on MAGMA flow simulation results. Through numerical modeling and experimental validation, Niu et al. [129] proposed the novel concept of Effective Flow Length (EFL) to precisely evaluate the castability of ultra-large thin-walled high-pressure die castings. This metric employs geometric stability and mechanical properties as critical criteria for structural-grade casting quality control.

4.3 Micro-scale simulation of die-casting Mg alloy

Microscale simulation of die-cast Mg alloys focuses on predicting grain morphology and size. Oldfield pioneered the integration of nucleation and growth functions into the heat source term of thermal transport equations, enabling quantitative characterization of solidification microstructures [174]. Current methodologies bifurcate into deterministic and stochastic approaches: deterministic methods describe grain nucleation density specific solidification at stages undercooling-dependent functions, while stochastic approaches employ probability-based models randomize nucleation sites and grain orientations. The microstructure modeling framework comprises coupled nucleation and growth models.

4.3.1 Grain nucleation model

Oldfield pioneered a continuous nucleation model that integrates undercooling and cooling rate effects to accurately characterize the complete nucleation process, enabling prediction of grain size distributions - hence termed the Oldfield Continuous Nucleation Model [174]. Hunt's instantaneous nucleation model (1980s), grounded in classical solidification theory, assumes immediate nucleation completion when the melt temperature drops below the nucleation temperature without subsequent nucleation events. While this simplification facilitates solid fraction calculation in micro-modeling, it fails to predict grain size accurately [175]. In contrast, Thevoz et al. [176] developed a quasi-instantaneous nucleation model incorporating Gaussian distribution, establishing a correlation between undercooling (ΔT) and stochastic density distribution for precise nucleation description. Grain density at specific undercooling is derived by integrating this probability distribution:

$$n(\Delta T) = n_{max} \Delta T_{\sigma} 2\pi \int 0\Delta T \exp(\Delta T - \Delta T_{N}) 2\Delta T_{\sigma} d(\Delta T)$$
(13)

where ΔT_N is the maximum supercooling degree of

nucleation, ΔT_{σ} is the standard deviation of the distribution, n_{max} is the maximum density of grains.

The model has been successfully applied to the simulation of dendritic and eutectic alloys, but the grain collision effect of the final phase is not considered.

4.3.2 Grain growth model

Grain growth models bifurcate into deterministic and stochastic categories. In deterministic models for eutectic alloys, grains are typically assumed to grow spherically. However, this assumption breaks down during late-stage solidification due to intergranular contacts, where evolving effective growth area alters growth kinetics. Dendritic alloy solidification exhibits greater complexity: dendritic growth governed by solute redistribution and diffusion depends not only on undercooling but also on constitutional undercooling, precluding simplistic spherical approximation. Consequently, Rappaz, Thevoz, and Kurz developed a dendritic growth kinetics model [177],[178]:

$$\frac{d}{dt} = \frac{1}{\pi \Gamma(k-1)} \left(\frac{1}{c_0}\right)^{\mu} \tag{14}$$

where R_g is the radius of the growing grain shell, D is the solute diffusion coefficient, m is the slope of the alloy liquidus, c_0 is the solute concentration in the liquid phase outside the spherical diffusion layer, Γ is the Gibbs-Thomson coefficient, k is the solute equilibrium distribution coefficient, c_R is the solute concentration in the liquid phase at the spherical inner diffusion layer. c_* is the solute concentration in the interdendritic liquid phase in the spherical grain.

Recognizing the limitations of deterministic solidification models in heat and mass transfer, necessitates stochastic approaches. In static systems, these processes exhibit diffusion-controlled nature, where diffusion is intrinsically a microscopic stochastic process. Furthermore, grain growth incorporates random characteristics such as energy fluctuations and structural perturbations. Predominant stochastic simulation methodologies currently include Monte Carlo (MC), Cellular Automata (CA), and Phase Field (PF) methods.

The Monte Carlo (MC) method developed by Spittle and Brown minimizes interfacial energy by computing energy states at heterogeneous interfaces and executing state transitions via stochastic probabilities. This approach constructs 2D microstructural models exhibiting exceptional consistency with metallographic sections, accurately replicating grain selection in columnar zones, Columnar-to-Equiaxed Transition (CET), and qualitatively demonstrating impacts of solute concentration and melt superheat on final microstructures

[179],[180]

Cellular Automata (CA) integrates strengths of stochastic and deterministic approaches, employing an interfacial state grid to delineate solid/liquid phases while quantifying undercooling and solute concentration effects. Its large grid scale and computational domain enable decoupled temperature/flow field solutions via finite element, finite difference, or Boltzmann methods, achieving macro-micro coupled solidification microstructure simulation with broad applicability [181].

The phase field method replaces explicit interface tracking with evolving phase field variables, concurrently solving phase field equations with energy and solute conservation equations to precisely simulate solidification microstructural evolution. This framework further couples with macroscopic flow and temperature fields to predict alloy microstructural development [182].

4.3.3 Application

To elucidate microstructural evolution mechanisms, numerical techniques such as Cellular Automata (CA) and phase field methods are extensively employed in dendritic growth studies. Huo et al. [183] developed a dual-grid CA model to simulate equiaxed and columnar grain growth during directional solidification of Mg-Al alloys. Böttger et al. [184] investigated equiaxed solidification in Mg-Al alloys using phase field modeling. As shown in Fig. 11, Wu et al. [185] performed numerical simulations of morphological characteristics and spatial distribution of Mg-Al eutectic structures in die-cast Mg alloys via a modified CA model, demonstrating excellent agreement with experimental observations.

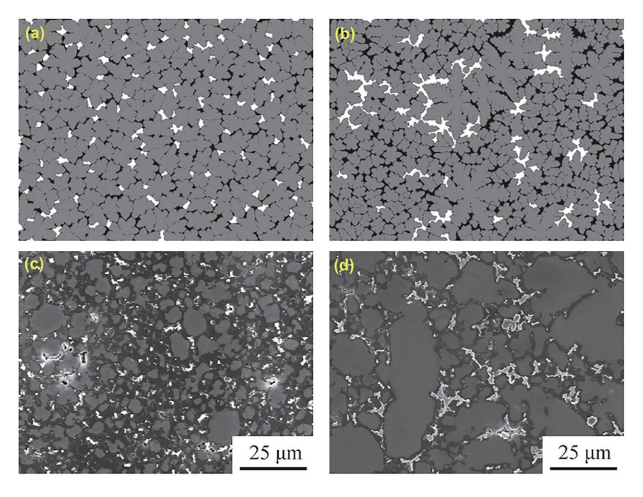


Fig.11 Distribution of Mg-Al eutectic at surface (a, c) and central (b, d) regions of "cover-plate" die casting: (a-b) simulated, (c-d) experimental observed [185].

Controlling cooling rates is critical for enhancing solidification microstructures in Mg alloys. Wang et al.

established a quantitative model describing synergistic effects of cooling rate and Zr content on heterogeneous nucleation efficiency in Mg-Gd-Y-Zr alloys, with CA-simulated grain size and eutectic phase volume fraction demonstrating excellent agreement with data. Through experimental experimental-numerical analysis, Zhao et al. [187] revealed that rapid cooling crucially refines grains by elevating effective undercooling and counteracting latent heat inhibition of heterogeneous nucleation. Integrating synchrotron radiation X-ray imaging with phase field simulations, Wang et al. [188] systematically investigated cooling rate effects on dendritic morphology evolution in Mg-Gd alloys under fixed thermal gradients. They discovered that low cooling rates dominate orientation selection, whereas high rates trigger splitting instability, governed by dynamic equilibrium between solute diffusion fields and interfacial energy anisotropy, as shown in Fig. 12.

During die casting, metal solidifies under applied pressure, which critically governs microstructural evolution in Mg alloys. Li et al. [189] employed cellular automata to simulate microstructure development and microsegregation under unidirectional pressure. Integrating thermodynamic calculations with polycrystalline phase-field modeling, Pan et al. [190] revealed a pressure threshold effect on dendritic growth in Mg-Al alloys.

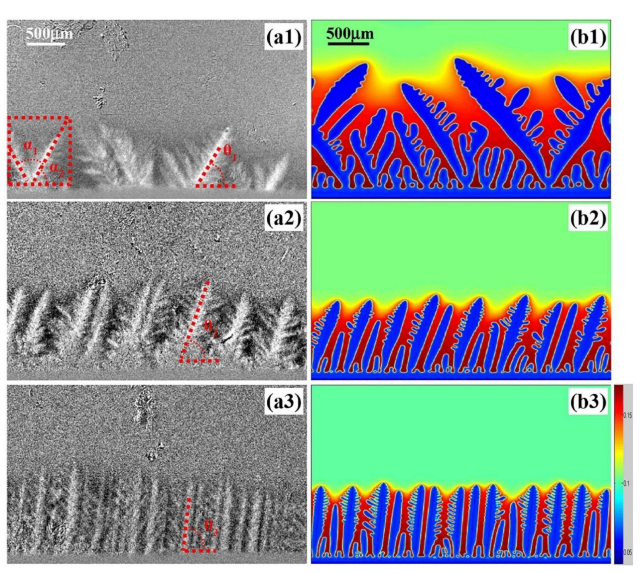


Fig.12 The dendritic morphology of Mg-6wt.%Gd alloy under three different cooling rates R = 0.033 K/s, R = 0.1 K/s, and R = 0.25 K/s in directional solidification from the top to bottom, respectively: experimental results (a1-a3), and simulated results (b1-b3) [188].

Although current simulations of solidification

microprocesses achieve close alignment with experimental results under laboratory conditions, the higher-order complexity of solidification mechanisms and process variables in industrial environments poses significant challenges.

4.4 Atomic-scale simulation of die-casting Mg alloy

Atomic-scale simulations serve pivotal theoretical tools for elucidating phase transformation mechanisms in die-cast Mg alloys. Lin et al. [191] demonstrated that Ca addition enhances the thermal stability of Al₂Ca precipitates in AZ91 alloy, revealing atomic-scale evolution mechanisms. Yang et al. [192] investigated aged high-pressure die-cast Mg-Al-RE alloys, determining key parameters for quantitative strengthening models via first-principles to refine theoretical frameworks. Furthermore, collaborative work by Yang and Lv et al. resolved long-standing debates by confirming the thermal stability of Al₁₁RE₃ phases through rigorous first-principles analysis [193],[194].

Atomic-scale simulations further elucidate complex solute segregation behaviors at grain boundaries. In Mg-Nd-Mn systems, large solute atoms Nd and small atoms Mn form four novel periodic asymmetric ordered segregation configurations at tilt grain boundaries. This phenomenon is governed by strain field distribution: molecular dynamics coupled with Voronoi topology analysis reveals periodically alternating tensile/compressive strain regions along linear tilt boundaries. Driven by elastic strain energy minimization, solute atoms selectively occupy specific lattice sites, demonstrating non-stochastic segregation behavior [195].

Die casting poses distinctive challenges, including rapid solidification, complex stress states, interactions. multicomponent Current modeling approaches require breakthroughs in cross-scale correlation, extreme non-equilibrium condition modeling, and high-precision multi-element potential functions. Integrative multiscale modeling combining machine learning, high-throughput computing, and advanced in situ characterization will be pivotal for the precision design and performance control of Mg alloy castings.

5 Die casting process and its effect on the properties of Mg alloy

Die casting processes are classified into conventional die casting (HPDC), vacuum die casting (VADC), semi-solid die casting (SSDC), and squeeze die casting (SDC), based on their underlying principles, equipment configurations, and material states. Notably,

VADC has evolved into a super vacuum die casting (SVDC) variant. Given the significant advantages of HPDC/VADC and the derived SVDC technology in enhancing casting integrity, particularly in reducing gas porosity and oxide inclusions and their emergence as a key development direction in critical fields like automotive lightweighting, this review focuses specifically on vacuum die casting (VADC/SVDC), detailing its fundamentals, characteristics, and key

HPDC and VADC have emerged as dominant technologies for commercial magnesium manufacturing due to their superior cost-effectiveness, dimensional accuracy, and surface quality [196]-[198]. VADC enhances casting integrity by evacuating the die cavity to 60-300 mbar before melt injection, while SVDC further reduces cavity pressure below 60 mbar via advanced control systems and high-efficiency vacuum pumps, achieving more effective defect suppression. This vacuum optimization significantly improves mechanical properties by reducing porosity-related defects, as demonstrated by Li et al. [199], showing 90% porosity reduction in AZ91D alloy with modified vacuum-assisted HPDC, as shown in Fig. 13. Le et al. [200] reported that grain refinement from rapid cooling in SVDC contributes 90% to strength enhancement in AE44 alloy. It also enhances heat-treatability by effectively suppressing surface blistering, enabling post-casting strengthening treatments [201]-[203]. Crucially, vacuum processes substantially optimize corrosion resistance [204]-[206]. Wen et al. [207] revealed that SVDC improves AM60B alloy's corrosion resistance by reducing the primary a-Mg phase volume fraction, thereby minimizing active-phase exposure and achieving significantly lower corrosion rates than HPDC. Current research predominantly focuses on alloy composition effects, whereas systematic comparative studies across die-casting processes and optimizations remain parametric critically underdeveloped, constituting a key constraint for high-end magnesium alloy applications.

Additionally, achieving ultra-low vacuum levels below 60 mbar remains a significant challenge in large-scale high-pressure die casting. The structural complexity and production scale of oversized castings impede the attainment of vacuum conditions equivalent to those for smaller components. This technological barrier is exemplified in the production of Tesla Model Y rear subframes, where VADC rather than SVDC is currently employed despite ongoing industry advancements in casting technologies.

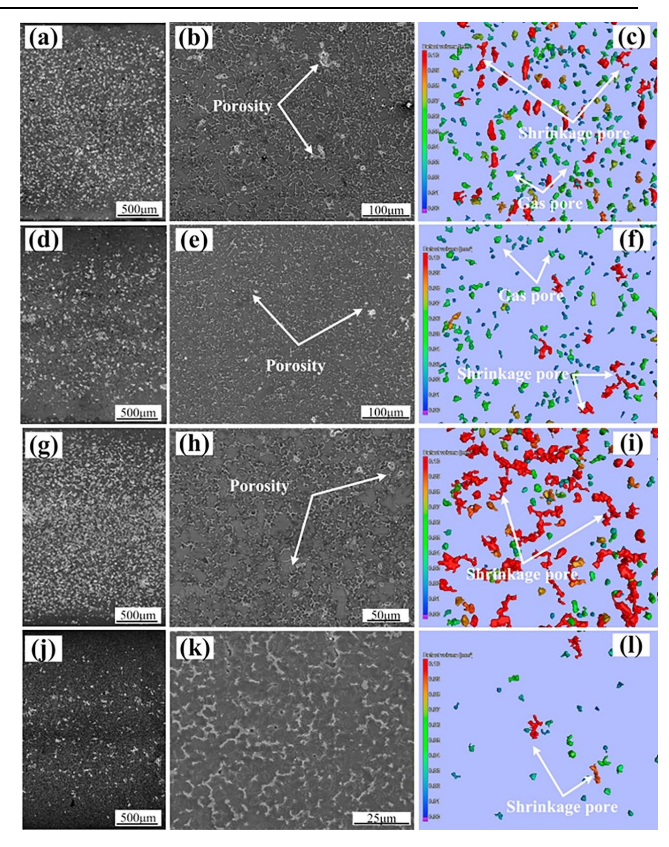


Fig.13 Comparison of microstructure (the first column: OM and second column: SEM) and porosity (the third column: X-Ray tomography) in the specimens of the conventional (the first row), vacuum-assist (the second row), modified vacuum-assist (the third row), and improved vacuum-assist (the fourth row) HPDC processes [199]

6 Summary and prospect

Integrated die casting technology demonstrates transformative advantages by consolidating multiple traditional components into single complex geometries, streamlining production, reducing costs, and enhancing structural stiffness and integration. The application of Mg alloys to this process represents a critical pathway to overcome lightweighting bottlenecks and meet future demands for high-performance lightweight structures in equipment. This review systematically advanced examines four key research dimensions: alloy design for integrated casting, characteristic defect formation mechanisms, implementation of numerical simulation, and process-performance relationships, establishing a holistic analytical framework linking process parameters, composition, defect genesis, simulation, and performance optimization. Future research should shift focus toward integrated multidisciplinary innovation encompassing materials, processes, equipment, simulation, performance to accelerate technological maturation and widespread industrial adoption

Reference

- Liu, X, Bie, Y, Chen, Z. Analysis of the Impact of the Development of New Energy Vehicles on Manufacturing Processes. Internal Combustion Engine & Parts, 2021, 208–209.
- [2] Su, H, Wang, J, Liu, C, Yan, C, et al. Uncovering the Damage Behavior of Heterogeneous Grains in Mg-RE Alloys. Eng. Fract. Mech. 2025, 318, 110967.
- [3] Tian, G, Wang, J, Zhang, C, Su, H, et al. Quantifying the Influence of Microstructure on the Corrosion of Mg-Li Alloys by Using X-Ray CT. Corros. Sci. 2024, 229, 111848.
- [4] Tian, G, Wang, J, Wang, S, Xue, C, et al. Achieving Ultra-High Stiffness by Solidifying and Precipitating Micro-Compounds in HCP/BCC Dual Matrix of a New Mg-Li Alloy. J. Alloys Compd. 2023, 964, 171324.
- [5] Ruden, T J. Structural Design Trends for Magnesium Die Casting. In *Production, Refining, Fabrication and Recycling of Light Metals*; Bouchard, M., Tremblay, P., Eds.; Proceedings of Metallurgical Society of Canadian Institute of Mining and Metallurgy; Pergamon: Oxford, 1990; pp 341–347.
- [6] Luo, A A. Magnesium Casting Technology for Structural Applications. J. Magnes. Alloys 2013, 1 (1), 2–22.
- [7] Weiler, J P. A Review of Magnesium Die-Castings for Closure Applications. J. Magnes. Alloys 2019, 7 (2), 297–304.
- [8] Li, Z, Li, D, Zhou, W, Hu, B, et al. Characterization on the Formation of Porosity and Tensile Properties Prediction in Die Casting Mg Alloys. J. Magnes. Alloys 2022, 10 (7), 1857–1867.
- [9] Giga Casting 2.0: Transforming Automotive Manufacturing stellarix.https://stellarix.com/insights/blogs/giga-casting-2-0-transfor
 - ming-automotive-manufacturing/ (accessed 2025-06-08).
- [10] Baser, T A, Umay, E, Akinci, V. New Trends in Aluminum Die Casting Alloys for Automotive Applications; 2022; Vol. 21, pp 79–87.
- [11] Li, T, Song, J, Zhang, A, You, G, et al. Progress and Prospects in Mg-Alloy Super-Sized High Pressure Die Casting for Automotive Structural Components. J. Magnes. Alloys 2023, 11 (11), 4166–4180.
- [12] Huang, J, Pan, W, Tang, X, Zhang, J, et al. Research Status and Progress of Integrated Die - Casting in the Automobile Industry. Heavy Cast. Forg. 2025, No. 02, 29–35.
- [13] Cha, M, Gu, T, Ma, P, Chen, Y, et al. Research Progress of Die - Casting Forming Technology for Large - Scale

- Integrated Structural Components of Light Alloys. *Special* Casting & Nonferrous Alloys, 2024, 44, 1009–1022.
- [14] Li, T, Wang, F, Du, X, Bai, S, et al. Effect of Al Content on Hot Tearing Susceptibility of Mg-5Zn-0.6Mn-xAl-0.6Zr Alloys. Int. J. Met. 2024, 18 (2), 1037-1051.
- [15] Hu, B, Li, D, Wang, J, Li, Z, et al. Hot Tearing Behavior in Double Ternary Eutectic Alloy System: Mg-Ce-Al Alloys. Metall. Mater. Trans. A 2020, 51 (12), 6658–6669.
- [16] Vinodh, G, Jafari Nodooshan, H R, Li, D, Zeng, X, et al. Effect of Al Content on Hot-Tearing Susceptibility of Mg-10Zn-xAl Alloys. Metall. Mater. Trans. A 2020, 51 (4), 1897–1910.
- [17] Marodkar, A S, Patil, H, Chavhan, J, Borkar, H. Effect of Gravity Die Casting, Squeeze Casting and Extrusion on Microstructure, Mechanical Properties and Corrosion Behaviour of AZ91 Magnesium Alloy. Mater. Today Proc. 2023.
- [18] Zhang, D, Zhang, D, Bu, F, Li, X, et al. Effects of Minor Sr Addition on the Microstructure, Mechanical Properties and Creep Behavior of High Pressure Die Casting AZ91-0.5RE Based Alloy. Mater. Sci. Eng. A 2017, 693, 51–59.
- [19] Rong, J, Xiao, W, Fu, Y, Zhao, X, et al. A High Performance Mg-Al-Ca Alloy Processed by High Pressure Die Casting: Microstructure, Mechanical Properties and Thermal Conductivity. Mater. Sci. Eng. A 2022, 849, 143500.
- [20] Zhang, J, Liu, K, Fang, D, Qiu, X, et al. Microstructures, Mechanical Properties and Corrosion Behavior of High-Pressure Die-Cast Mg-4Al-0.4Mn-xPr (x = 1, 2, 4, 6) Alloys. J. Alloys Compd. 2009, 480 (2), 810–819.
- [21] Hu, H, Zhou, M, Sun, Z, Li, N. Tensile Behaviour and Fracture Characteristics of Die Cast Magnesium Alloy AM50. J. Mater. Process. Technol. 2008, 201 (1), 364–368
- [22] Ji, S, Yang, W, Jiang, B, Patel, J B, et al. Weibull Statistical Analysis of the Effect of Melt Conditioning on the Mechanical Properties of AM60 Alloy. Mater. Sci. Eng. A 2013, 566, 119–125.
- [23] Zhu, S, Abbott, T B, Nie, J-F, Ang, H Q, et al. Re-Evaluation of the Mechanical Properties and Creep Resistance of Commercial Magnesium Die-Casting Alloy AE44. J. Magnes. Alloys 2021, 9 (5), 1537–1545.
- [24] Lv, S, Lü, X, Meng, F, Yang, Q, et al. Microstructures and Mechanical Properties in a Gd-Modified High-Pressure Die Casting Mg-4Al-3La-0.3Mn Alloy. Mater. Sci. Eng. A 2020, 773, 138725.
- [25] Luo, W, Yin, W-L, Li, Y-H, Dai, J, et al. Research on

- Microstructure and Mechanical Properties of Die Casting Mg-4Al-1Si-3RE (Ce, La) and AS41 Alloys. Mater. Today Commun. 2022, 33, 104625.
- [26] Zhang, D, Li, B, Zhang, J, Niu, T, et al. Influence of Minor RE Addition on Microstructures, Tensile Properties, and Creep Resistance in a Die-Cast Mg-Al-Ca-Mn Alloy. J. Mater. Res. Technol. 2023, 26, 3136-3145.
- [27] Baril, E, Labelle, P, Pekguleryuz, M. Elevated Temperature Mg-Al-Sr: Creep Resistance, Mechanical Properties, and Microstructure. JOM 2003, 55 (11), 34–39.
- [28] Pekgüleryüz, M Ö, Avedesian, M M. Magnesium Alloying, Some Potentials for Alloy Development. J. Jpn. Inst. Light Met. 1992, 42 (12), 679–686.
- [29] Li, B, Zhang, J, Ye, F, Tang, R, et al. An Approach to Studying the Hot Tearing Mechanism of Alloying Elements in Ternary Mg-Zn-Al Alloys. J. Mater. Process. Technol. 2023, 317, 117980.
- [30] Song, J, Pan, F, Jiang, B, Atrens, A, et al. A Review on Hot Tearing of Magnesium Alloys. J. Magnes. Alloys 2016, 4 (3), 151–172.
- [31] Anyanwu, I A, Gokan, Y, Nozawa, S, Suzuki, A, et al. Development of New Die-Castable Mg-Zn-Al-Ca-RE Alloys for High Temperature Applications. Mater. Trans. 2003, 44 (4), 562–570.
- [32] Zhang, Z, Couture, A, Luo, A. An Investigation of the Properties of Mg-Zn-Al Alloys. Scr. Mater. 1998, 39 (1), 45–53.
- [33] Xiao, W, Jia, S, Wang, L, Wu, Y, et al. The Microstructures and Mechanical Properties of Cast Mg–Zn–Al–RE Alloys. J. Alloys Compd. 2009, 480 (2), L33–L36.
- [34] Lv, S, Xie, Z, Yang, Q, Meng, F, et al. Microstructures and Mechanical Properties of a Hot-Extruded Mg-8Zn-6Al-1Gd (Wt%) Alloy. J. Alloys Compd. 2022, 904, 164040.
- [35] Lv, S, Yang, Q, Lv, X, Meng, F, et al. Intermetallic Phases and Mechanical Properties of a Mg–8Zn–6Al–1Sm (Wt%) Casting Alloy. Mater. Sci. Eng. A 2022, 852, 143719.
- [36] Vogel, M, Kraft, O, Dehm, G, Arzt, E. Quasi-Crystalline Grain-Boundary Phase in the Magnesium Die-Cast Alloy ZA85. Scr. Mater. 2001, 45 (5), 517–524.
- [37] Shi, Z-Z, Zhang, W-Z. A Transmission Electron Microscopy Investigation of Crystallography of τ-Mg32(Al, Zn)49 Precipitates in a Mg–Zn–Al Alloy. Scr. Mater. 2011, 64 (2), 201–204.
- [38] Sun, W, Lincoln, F J, Sugiyama, K, Hiraga, K. Structure Refinement of (Al, Zn)49Mg32-Type Phases by Single-Crystal X-Ray Diffraction. Mater. Sci. Eng. A 2000, 294–296, 327–330.

- [39] Zheng, Y, Bourgeois, L, Nie, J-F. Aperiodic Structures of Rod-Shaped Precipitates in a Mg-Zn-Al Alloy. Scr. Mater. 2021, 205, 114189.
- [40] Huang, J, Pan, W, Tang, X, Zhang, J, et al. Research Status and Progress of Integrated Die - Casting in the Automobile Industry. Heavy Cast. Forg. 2025, No. 02, 29–35
- [41] Zheng, F, Weng, K, Zhang, C, Li, L,et al. Effects of Sr and B on Solidification Range and Flowability of AZ91 Magnesium Alloy. Foundry 2008, No. 02, 170–172.
- [42] Yim, C D, You, B S, Jang, R S, Lim, S G. Effects of Melt Temperature and Mold Preheating Temperature on the Fluidity of Ca Containing AZ31 Alloys. J. Mater. Sci. 2006, 41 (8), 2347–2350.
- [43] Srinivasan, A, Pillai, U T S, Pai, B C. Effect of Pb Addition on Ageing Behavior of AZ91 Magnesium Alloy. Mater. Sci. Eng. A 2007, 452–453, 87–92.
- [44] Wang, Y, Fu, J, Yang, Y. Effect of Nd Addition on Microstructures and Mechanical Properties of AZ80 Magnesium Alloys. Trans. Nonferrous Met. Soc. China 2012, 22 (6), 1322–1328.
- [45] Cui, P, Hu, M, Ji, Z, Xu, H, et al. Effect of La/Nd Ratio on Precipitation Kinetics and Tensile Properties of Squeeze-Cast Mg-Al-Zn-La-Nd Alloys. Mater. Today Commun. 2022, 33, 104710.
- [46] Eftekhar, A H, Sadrossadat, S M, Reihanian, M. Microstructural Investigation and High Temperature Mechanical Behavior of AXE622 Cast Mg Alloy. Met. Mater. Int. 2022, 28 (5), 1062–1074.
- [47] Nami, B, Razavi, H, Mirdamadi, S, Shabestari, S G, et al. Effect of Ca and Rare Earth Elements on Impression Creep Properties of AZ91 Magnesium Alloy. Metall. Mater. Trans. A 2010, 41 (8), 1973–1982.
- [48] Wu, G, Fan, Y, Gao, H, Zhai, C, et al. The Effect of Ca and Rare Earth Elements on the Microstructure, Mechanical Properties and Corrosion Behavior of AZ91D. Mater. Sci. Eng. A 2005, 408 (1), 255–263.
- [49] Gariboldi, E, Lo Conte, A. Evaluation of Toughness Characteristics of a Die-Cast Mg-Al-Mn Alloy Am60B under Different Microstructural Conditions. Mater. Sci. Eng. A 2004, 387–389, 34–40.
- [50] Song, J, Xiong, S-M, Li, M, Allison, J. The Correlation between Microstructure and Mechanical Properties of High-Pressure Die-Cast AM50 Alloy. J. Alloys Compd. 2009, 477 (1), 863–869.
- [51] Sharifi, P, Fan, Y, Anaraki, H B, Banerjee, A, et al. Evaluation of Cooling Rate Effects on the Mechanical Properties of Die Cast Magnesium Alloy AM60. Metall. Mater. Trans. A 2016, 47 (10), 5159–5168.

- [52] Weiler, J P, Wood, J T, Klassen, R J, Berkmortel, R, et al. Stress-Strain Response in Skin and Core Regions of Die Cast Magnesium Alloy AM60B Determined from Spherical Microindentation; 2005; pp 191–196.
- [53] Biswas, S, Sket, F, Chiumenti, M, Gutiérrez-Urrutia, I, et al. Relationship Between the 3D Porosity and β-Phase Distributions and the Mechanical Properties of a High Pressure Die Cast AZ91 Mg Alloy. Metall. Mater. Trans. A 2013, 44 (9), 4391–4403.
- [54] Zhang, Y, Zheng, J, Shou, H, Li, J, et al. The Gradient Microstructure and Deformation Heterogeneity in HPDC AM60 Alloy. Mater. Sci. Eng. A 2020, 792, 139647.
- [55] Sevik, H, Açıkgöz, S, Can Kurnaz, S. The Effect of Tin Addition on the Microstructure and Mechanical Properties of Squeeze Cast AM60 Alloy. J. Alloys Compd. 2010, 508 (1), 110–114.
- [56] Homma, T, Nakawaki, S, Kamado, S. Improvement in Creep Property of a Cast Mg–6Al–3Ca Alloy by Mn Addition. Scr. Mater. 2010, 63 (12), 1173–1176.
- [57] Luo, A, Pekguleryuz, M O. Cast Magnesium Alloys for Elevated Temperature Applications. J. Mater. Sci. 1994, 29 (20), 5259–5271.
- [58] Dargusch, M S, Shi, Z, Zhu, H, Atrens, A, et al. Microstructure Modification and Corrosion Resistance Enhancement of Die-Cast Mg-Al-Re Alloy by Sr Alloying. J. Magnes. Alloys 2021, 9 (3), 950–963.
- [59] Bichler, L, Ravindran ,C., and Sediako, D. Onset of Hot Tearing in AE42 Magnesium Alloy. Can. Metall. Q. 2009, 48 (1), 81–89.
- [60] Powell, B R, Rezhets, V, Balogh, M P, Waldo, R A. Microstructure and Creep Behavior in AE42 Magnesium Die-Casting Alloy. JOM 2002, 54 (8), 34–38.
- [61] Bakke, P, Westengen, H. The Role of Rare Earth Elements in Structure and Property Control of Magnesium Die Casting Alloys; 2005; pp 291–296.
- [62] Easton, M, Gibson, M, Zhu, S M, Yang, K, et al. Achievements in Magnesium Alloy Research; 2015; Vol. 828–829, pp 3–8.
- [63] Liu, B, Yang, J, Zhang, X, Yang, Q, et al. Development and Application of Magnesium Alloy Parts for Automotive OEMs: A Review. J. Magnes. Alloys 2023, 11 (1), 15–47.
- [64] Zhu, S, Easton, M A, Abbott, T B, Nie, J-F, et al. Evaluation of Magnesium Die-Casting Alloys for Elevated Temperature Applications: Microstructure, Tensile Properties, and Creep Resistance. Metall. Mater. Trans. A 2015, 46 (8), 3543–3554.
- [65] Zhang, J, Zhang, M, Meng, J, Wu, R, et al. Microstructures and Mechanical Properties of

- Heat-Resistant High-Pressure Die-Cast Mg–4Al–xLa–0.3Mn (*x*= 1, 2, 4, 6) Alloys. Mater. Sci. Eng. A 2010, 527 (10), 2527–2537.
- [66] Zhang, J, Leng, Z, Zhang, M, Meng, J, et al. Effect of Ce on Microstructure, Mechanical Properties and Corrosion Behavior of High-Pressure Die-Cast Mg-4Al-Based Alloy. J. Alloys Compd. 2011, 509 (3), 1069–1078.
- [67] Evangelista, E, Gariboldi, E, Lohne, O, Spigarelli, S. High-Temperature Behaviour of as Die-Cast and Heat Treated Mg-Al-Si AS21X Magnesium Alloy. Mater. Sci. Eng. A 2004, 387–389, 41–45.
- [68] Blum, W, Zhang, P, Watzinger, B, Grossmann, B v, et al. Comparative Study of Creep of the Die-Cast Mg-Alloys AZ91, AS21, AS41, AM60 and AE42. Mater. Sci. Eng. A 2001, 319–321, 735–740.
- [69] Wu, H-D, Du, J, Dou, Q, Li, W. Effects of Strontium on Modification of Primary Mg 2Si Phases in Hypereutectic Mg-Si Alloy. Zhuzao/Foundry 2011, 60 (4), 368–371.
- [70] Pei-wei, S. Effects of Sb Addition on Microstructure and Mechanical Properties of Mg-4Al-4Si Magnesium Alloy. Hot Work. Technol. 2012.
- [71] Chang Shin, H, Son, J, Min, B K, Choi, Y S, et al. The Effect of Ce on the Modification of Mg2Si Phases of As-Cast Eutectic Mg-Si Alloys. J. Alloys Compd. 2019, 792, 59–68.
- [72] Han, W, Li, K, Hu, F, Li, Y, et al. Microstructure and Mechanical Properties of Mg-2.5Si-xCe in-Situ Particle Reinforced Composites Prepared by Rapid Solidification Process. Results Phys. 2019, 15, 102509.
- [73] Abaspour, S, Cáceres, C H. Thermodynamics-Based Selection and Design of Creep-Resistant Cast Mg Alloys. Metall. Mater. Trans. A 2015, 46 (12), 5972–5988.
- [74] Ganguly, S, Mondal, A K. Influence of SiC Nanoparticles Addition on Microstructure and Creep Behavior of Squeeze-Cast AZ91-Ca-Sb Magnesium Alloy. Mater. Sci. Eng. A 2018, 718, 377–389.
- [75] Cao, G, Kou, S. Hot Tearing of Ternary Mg-Al-Ca Alloy Castings. Metall. Mater. Trans. A 2006, 37 (12), 3647–3663.
- [76] Zhu, S M, Nie, J F, Mordike, B L. Creep and Rupture Properties of a Squeeze-Cast Mg-Al-Ca Alloy. Metall. Mater. Trans. A 2006, 37 (4), 1221–1229.
- [77] Min, X, Du, W, Xue, F, Sun, Y. Phenomenon of Ca Increasing the Melting Point of Mg17Al12 Phase and Its Analysis by EET Theory. Chin. Sci. Bull. 2002, 47 (2), 109–112.
- [78] Chen, G, Peng, X, Fan, P, Xie, W, et al. Effects of Sr and Y on Microstructure and Corrosion Resistance of AZ31 Magnesium Alloy. Trans. Nonferrous Met. Soc. China

- 2011, 21 (4), 725-731.
- [79] Hirai, K, Somekawa, H, Takigawa, Y, Higashi, K. Effects of Ca and Sr Addition on Mechanical Properties of a Cast AZ91 Magnesium Alloy at Room and Elevated Temperature. Mater. Sci. Eng. A 2005, 403 (1), 276–280.
- [80] Mordike, B L. Creep-Resistant Magnesium Alloys. Mater. Sci. Eng. A 2002, 324 (1), 103–112.
- [81] Pekguleryuz, M O, Baril, E. Development of Creep Resistant Mg-Al-Sr Alloys. In *Essential Readings in Magnesium Technology*; Mathaudhu, S. N., Luo, A. A., Neelameggham, N. R., Nyberg, E. A., Sillekens, W. H., Eds.; Springer International Publishing: Cham, 2016; pp 283–289.
- [82] Labelle, P, Pekguleryuz, M O, Argo, D, Dierks, M, et al. Heat Resistant Magnesium Alloys for Power-Train Applications. SAE Trans. 2001, 110, 423–430.
- [83] Pekguleryuz, M, Labelle, P, Argo, D. Magnesium Die Casting Alloy AJ62x with Superior Creep Resistance, Ductility and Die Castability; SAE International, 2003.
- [84] CHADHA, G, ALLISON, J E, JONES, J W. The Role of Microstructure on Ductility of Die-Cast AM50 and AM60 Magnesium Alloys. Metall. Mater. Trans. A 2007, 38 (2), 286–297.
- [85] Jung, I Y. Prediction of Tensile Ductility in Porous Materials. Philos. Mag. A 2002, 82 (11), 2263–2268.
- [86] Brown, L M, Embury, J D. INITIATION AND GROWTH OF VOIDS AT SECOND PHASE PARTICLES.; 1973; Vol. 1, pp 164–169.
- [87] Hou, Q, Wu, X, Li, Z, Feng, S, et al. Artificial Intelligence Enabled Microstructure Prediction in Al Alloy Castings. J. Mater. Sci. Technol. 2026, 241, 21–34.
- [88] Miao, Y, Li, Z, Wu, X, Feng, S, et al. Identifying the Critical Micropores Characteristics for the Degradation of Mechanical Properties in Automotive Wheels. J. Mater. Res. Technol. 2025, 36, 8075–8087.
- [89] Zhang, Y, Xue, C, Wang, J, Yang, X, et al. Quantifying the Effects of Hydrogen Concentration and Cooling Rates on Porosity Formation in Al–Li Alloys. J. Mater. Res. Technol. 2023, 26, 1938–1954.
- [90] Zhang, Y, Xue, C, Yang, X, Li, X, et al. Uncovering the Effects of Local Pressure and Cooling Rates on Porosity Formation in AA2060 Al-Li Alloy. Mater. Today Commun. 2023, 35, 106384.
- [91] Wu, M, Hou, Y, Hua, L, Ma, H, et al. On the Deformation Behavior of Heterogeneous Microstructure and Its Effect on the Mechanical Properties of Die Cast AZ91D Magnesium Alloy. J. Magnes. Alloys 2022, 10 (7), 1981–1993.
- [92] Yang, Z, Maurey, A, Kang, J, Wilkinson, D S. 2D and 3D

- Characterization of Pore Defects in Die Cast AM60. Mater. Charact. 2016, 114, 254–262.
- [93] Li, X, Xiong, S M, Guo, Z. Correlation between Porosity and Fracture Mechanism in High Pressure Die Casting of AM60B Alloy. J. Mater. Sci. Technol. 2016, 32 (1), 54–61.
- [94] Hou, Y, Wu, M, Tian, B, Li, X, et al. Characteristics and Formation Mechanisms of Defect Bands in Vacuum-Assisted High-Pressure Die Casting AE44 Alloy. Trans. Nonferrous Met. Soc. China 2022, 32 (6), 1852–1865.
- [95] Dahle, A K, Sannes, S, St. John, D H, Westengen, H. Formation of Defect Bands in High Pressure Die Cast Magnesium Alloys. J. Light Met. 2001, 1 (2), 99–103.
- [96] Wu, M, Hou, Y, Li, X, Xiong, S, et al. Microstructure Characteristics and Formation Mechanism of Defect Bands in Die - Cast Magnesium Alloys. Spec. Cast. Nonferrous Alloys 2020, 40 (02), 117–122.
- [97] Cao, H, Sun, Q, Pu, Q, Wang, L, et al. Effect of Vacuum Degree and T6 Treatment on the Microstructure and Mechanical Properties of Al–Si–Cu Alloy Die Castings. Vacuum 2020, 172, 109063.
- [98] Cao, H, Hao, M, Shen, C, Liang, P. The Influence of Different Vacuum Degree on the Porosity and Mechanical Properties of Aluminum Die Casting. Vacuum 2017, 146, 278–281.
- [99] Kang, H, Jang, H, Oh, S-H, Yoon, P, et al. Effects of Gate System Design on Pore Defects and Mechanical Properties of Pore-Free Die-Cast Al-Si-Cu Alloy. Mater. Today Commun. 2022, 31, 103673.
- [100] Zhang, T, Yu, W, Ma, C, Chen, W, et al. The Effect of Different High Pressure Die Casting Parameters on 3D Microstructure and Mechanical Properties of AE44 Magnesium Alloy. J. Magnes. Alloys 2023, 11 (9), 3141–3150.
- [101] Li, S, Li, D, Zeng, X, Ding, W. Microstructure and Mechanical Properties of Mg-6Gd-3Y-0.5Zr Alloy Processed by High-Vacuum Die-Casting. Trans. Nonferrous Met. Soc. China 2014, 24 (12), 3769-3776.
- [102] Li, X, Yu, W, Wang, J, Xiong, S. Influence of Melt Flow in the Gating System on Microstructure and Mechanical Properties of High Pressure Die Casting AZ91D Magnesium Alloy. Mater. Sci. Eng. A 2018, 736, 219–227.
- [103] Li, X, Yu, W, Wang, J, Xiong, S. Influence of Melt Flow in the Gating System on Microstructure and Mechanical Properties of High Pressure Die Casting AZ91D Magnesium Alloy. Mater. Sci. Eng. A 2018, 736, 219–227.

- [104] Li, T, Davies, J M T, Luo, D. Consumption of Entrained Gases Within Bifilms During a Mg-Alloy Casting Process. Metall. Mater. Trans. B 2021, 52 (5), 3093–3106.
- [105] Yu, B, Jia, Z, Li, Y, Fu, L, et al. Research Progress of Magnesium - Alloy Melt Purification Technology. Foundry Technol. 2021, 42 (07), 635-643+650.
- [106] Griffiths, W D, Lai, N-W. Double Oxide Film Defects in Cast Magnesium Alloy. Metall. Mater. Trans. A 2007, 38 (1), 190–196.
- [107] Raiszadeh, R, Griffiths, W D. The Effect of Holding Liquid Aluminum Alloys on Oxide Film Content. Metall. Mater. Trans. B 2011, 42 (1), 133–143.
- [108] Cashion, S P, Ricketts, N J, Hayes, P C. The Mechanism of Protection of Molten Magnesium by Cover Gas Mixtures Containing Sulphur Hexafluoride. J. Light Met. 2002, 2 (1), 43–47.
- [109] Cashion, S P, Ricketts, N J, Hayes, P C. Characterisation of Protective Surface Films Formed on Molten Magnesium Protected by Air/SF6 Atmospheres. J. Light Met. 2002, 2 (1), 37–42.
- [110] Pettersen, G, Øvrelid, E, Tranell, G, Fenstad, J, et al. Characterisation of the Surface Films Formed on Molten Magnesium in Different Protective Atmospheres. Mater. Sci. Eng. A 2002, 332 (1), 285–294.
- [111] Peng, L, Zeng, G, Su, T C, Yasuda, H, et al. Al8Mn5 Particle Settling and Interactions with Oxide Films in Liquid AZ91 Magnesium Alloys. JOM 2019, 71 (7), 2235–2244.
- [112] Dispinar, D, and Campbell, J. Use of Bifilm Index as an Assessment of Liquid Metal Quality. Int. J. Cast Met. Res. 2006, 19 (1), 5–17.
- [113] Du, X, Wang, F, Wang, Z, Zhou, L, et al. Effect of Addition of Minor Amounts of Sb and Gd on Hot Tearing Susceptibility of Mg-5Al-3Ca Alloy. J. Magnes. Alloys 2023, 11 (2), 694–705.
- [114] Zhou, Y, Mao, P, Zhou, L, Wang, Z, et al. Effect of Long-Period Stacking Ordered Phase on Hot Tearing Susceptibility of Mg-1Zn-xY Alloys. J. Magnes. Alloys 2020, 8 (4), 1176–1185.
- [115] Pekguleryuz, M O, Kaya, A A. Magnesium Diecasting Alloys for High Temperature Applications. In *Essential Readings in Magnesium Technology*; Mathaudhu, S. N., Luo, A. A., Neelameggham, N. R., Nyberg, E. A., Sillekens, W. H., Eds.; Springer International Publishing: Cham, 2016; pp 297–303.
- [116] Cao, H, Huang, M, Wang, C, Long, S, et al. Research Status and Prospects of Melt Refining and Purification Technology of Magnesium Alloys. J. Magnes. Alloys

- 2019, 7 (3), 370–380.
- [117] El-Kaddah, N, Patel, A D, Natarajan, T T. The Electromagnetic Filtration of Molten Aluminum Using an Induced-Current Separator. JOM 1995, 47 (5), 46–49.
- [118] Eskin, G I. Broad Prospects for Commercial Application of the Ultrasonic (Cavitation) Melt Treatment of Light Alloys. Ultrason. Sonochem. 2001, 8 (3), 319–325.
- [119] Balasubramani, N, Wang, G, Easton, M A, StJohn, D H, et al. A Comparative Study of the Role of Solute, Potent Particles and Ultrasonic Treatment during Solidification of Pure Mg, Mg–Zn and Mg–Zr Alloys. J. Magnes. Alloys 2021, 9 (3), 829–839.
- [120] Kumar, A, Pandey, P M. Effect of Ultrasonic Assisted Sintering on Mechanical Properties and Degradation Behaviour of Mg15Nb3Zn1Ca Biomaterial. J. Magnes. Alloys 2021, 9 (6), 1989–2008.
- [121] Shao, Z, Le, Q, Cui, J, Zhang, Z. Numerical Simulation of Standing Waves for Ultrasonic Purification of Magnesium Alloy Melt. Trans. Nonferrous Met. Soc. China 2010, 20, s382–s387.
- [122] Khosro Aghayani, M, Niroumand, B. Effects of Ultrasonic Treatment on Microstructure and Tensile Strength of AZ91 Magnesium Alloy. J. Alloys Compd. 2011, 509 (1), 114–122.
- [123] Wang, J, Zhou, J, Tong, W, Yang, Y. Effect of Purification Treatment on Properties of Mg-Gd-Y-Zr Alloy. Trans. Nonferrous Met. Soc. China 2010, 20 (7), 1235–1239
- [124] Zha, J L, Xu, S Y, You, G Q, Long, S Y. A Continuous Fluxless Purification Technique for Mg Scrap Melt. Adv. Mater. Res. 2011, 295, 2151–2154.
- [125] Feng, Y, Liao, D, Chen, T. Confluence and Cold Shut Computation Based on Time Field in Casting Simulation. China Foundry 2021, 18 (2), 101–109.
- [126] Bharambe, C, Jaybhaye, M D, Dalmiya, A, Daund, C, et al. Analyzing Casting Defects in High-Pressure Die Casting Industrial Case Study. Mater. Today Proc. 2023, 72, 1079–1083.
- [127] Chen, T-Y, Wang, Y-C, Huang, C-F, Liu, Y-C, et al. Formation Mechanism and Improved Remedy of Thermal Property of Cold Shut Surface Defects in Vortex Flow Meters: Numerical Simulation and Experimental Verification in Investment Casting of 316 L Stainless Steel. J. Manuf. Process. 2024, 120, 542–554.
- [128] Wang, F, Guo, Z, Chen, Z. Optimization of Die Casting Process for Automobile Clutch Housings and Control of Cold Shut Defects. Met. Work. Hot Work. 2017, No. 19, 12–13.
- [129] Niu, Z, Liu, G, Li, T, Ji, S. Effect of High Pressure Die

- Casting on the Castability, Defects and Mechanical Properties of Aluminium Alloys in Extra-Large Thin-Wall Castings. J. Mater. Process. Technol. 2022, 303, 117525.
- [130] Lin, Q. Defects and Analysis of Die Castings. Mould Manuf. 2005, No. 12, 53-56+73.
- [131] Akhtar, S, Liu, Y, Wang, P, He, Z, et al. Understanding the Formation Mechanism of Defect Bands through ESCs Evolution in Non-Heat-Treated High-Pressure Die-Cast AlSi9MnVZr Alloy: Role of Shot Speeds and Intensification Pressure. J. Mater. Process. Technol. 2025, 341, 118915.
- [132] Lv, H, Tan, J, Geng, T, Wang, H, et al. Advances in High-Strength and High-Thermal Conductivity Cast Magnesium Alloys: Strategies for Property Optimization. J. Alloys Compd. 2025, 1029, 180843.
- [133] Wu, H B, Fan, Z T, Huang, N Y, Dong, X P, et al. Mold-Filling Characteristics of AZ91 Magnesium Alloy in the Low-Pressure Expendable Pattern Casting Process. J. Mater. Eng. Perform. 2005, 14 (1), 132–135.
- [134] Tunçay, T, Baytar, F, Tunçay, B, Sunar, T, et al. Effects of Mold Cavity Geometry on Flow Rate and Mechanical Properties in Al-Si-Mg Alloy. J. Mater. Eng. Perform. 2023, 32 (10), 4702–4711.
- [135] Cavaliere, G, Borgianni, Y, Savio, E. Performances of an In-Line Deep Learning-Based Inspection System for Surface Defects of Die-Cast Components for Hybrid Vehicles. Procedia CIRP 2024, 126, 999–1004.
- [136] Kazup, Á, Garami, A, Gácsi, Z. Prediction of the Tensile Properties of A356 Casted Alloy Based on the Pore Structure Using Machine Learning. Mater. Sci. Eng. A 2025, 935, 148338.
- [137] Rosnitschek, T, Erber, M, Alber-Laukant, B, Hartmann, C, et al. Predicting the Solidification Time of Low Pressure Die Castings Using Geometric Feature-Based Machine Learning Metamodels. Procedia CIRP 2023, 118, 1102–1107.
- [138] Han, H, Li, X, Cao, D, Wu, H. Defect Analysis and Countermeasures for Aluminum Alloy Die Castings and New Development of Die Casting Technology. Mech. Electr. Technol. 2014, No. 06, 95–97.
- [139] Xu, H, Liu, W, Wang, Y, Ma, S, et al. Control and Optimization of Defects in Die Casting of Complicated Right Crankcase Cover. J. Mater. Res. Technol. 2024, 33, 2831–2840.
- [140] Huang, H, Wang, Y X, Fu, P H, Peng, L M, et al. Fluidity of AZ91D and Mg-3Nd-0·2Zn-Zr (Wt-%) Magnesium Alloys: Response to Pouring and Mould Temperature. Int. J. Cast Met. Res. 2013, 26 (4), 213–219.

- [141] Li, Y, Wu, G, Chen, A, Liu, W, et al. Effects of Processing Parameters and Addition of Flame-Retardant into Moulding Sand on the Microstructure and Fluidity of Sand-Cast Magnesium Alloy Mg-10Gd-3Y-0.5Zr. J. Mater. Sci. Technol. 2017, 33 (6), 558–566.
- [142] Shankar, S, Apelian, D. Die Soldering: Mechanism of the Interface Reaction between Molten Aluminum Alloy and Tool Steel. Metall. Mater. Trans. B 2002, 33 (3), 465–476.
- [143] Chen, Z W. Formation and Progression of Die Soldering during High Pressure Die Casting. Mater. Sci. Eng. A 2005, 397 (1), 356–369.
- [144] Monroe, A, Sanders, P. The Need for a New Approach to Soldering in High Pressure Die Casting. Int. J. Met. 2021, 15 (2), 391–397.
- [145] Terek, P, Kovačević, L, Miletić, A, Panjan, P, et al. Effects of Die Core Treatments and Surface Finishes on the Sticking and Galling Tendency of Al–Si Alloy Casting during Ejection. Wear 2016, 356–357, 122–134.
- [146] Bowles, A L, Han, Q, Horton, J A. Castability of Magnesium Alloys. In *Essential Readings in Magnesium Technology*; Mathaudhu, S. N., Luo, A. A., Neelameggham, N. R., Nyberg, E. A., Sillekens, W. H., Eds.; Springer International Publishing: Cham, 2016; pp 187–192.
- [147] Han, J, Lu, H, Zhang, J, Ma, X, et al. Ideas for Handling Flash and Burrs of Die Casting Products. In *In Proceedings of the 2024 Chongqing Foundry Annual Conference*; Chongqing Hanli Machinery Manufacturing Co;, 2024; pp 283–284.
- [148] Princely, F L, Selvaraj, T. Vision Assisted Robotic Deburring of Edge Burrs in Cast Parts. Procedia Eng. 2014, 97, 1906–1914.
- [149] Onstein, I F, Bjerkeng, M, Martinsen, K. Automated Tool Trajectory Generation for Robotized Deburring of Cast Parts Based on 3D Scans. Procedia CIRP 2023, 118, 507–512.
- [150] Motoyama, Y, Sekiguchi, S, Okane, T, Yoshida, M. Thermo-Elasto-Plastic Finite Element Analysis of Warping Deformation during Casting of Gray Cast Iron. J. Mater. Process. Technol. 2020, 277, 116454.
- [151] Wang Fu, M, Zheng, J-Y. Die Casting for Fabrication of Metallic Components and Structures. In *Encyclopedia of Materials: Metals and Alloys*; Caballero, F. G., Ed.; Elsevier: Oxford, 2022; pp 54–72.
- [152] Vispute, P, Chaudhari, D. Utilizing Flow Simulation in the Design Phase of a Casting Die to Optimize Design Parameters and Defect Analysis. Mater. Today Proc. 2017, 4 (8), 9256–9263.

- [153] Zhang, J, Li, X, Xu, D, Yang, R. Recent Progress in the Simulation of Microstructure Evolution in Titanium Alloys. Prog. Nat. Sci. Mater. Int. 2019, 29 (3), 295–304.
- [154] Wang, S, Li, Z, Qiao, H, Hou, Q, et al. Multi-Scale Fatigue Life Prediction Method of the A356 Wheel Considering the Effects of Casting Microstructure. Int. J. Fatigue 2025, 198, 108977.
- [155] Wang, S, Li, Z, Ma, X, Wu, X, et al. Integrated Predictions of the Influence of Mesh Size, Casting Defects and SDAS on the Fatigue Life of Aluminum Alloy Wheels. J. Mater. Res. Technol. 2025, 35, 3956–3967.
- [156] Ransing, R S. Review of Optimization Methods for Casting Simulation; 2005.
- [157] M, B K. A Look Back at the 20th Century. Part II. Casting Process Simulation. Mod. Cast. 2000, 90 (12), 43–45.
- [158] Yang, J, Liu, B, Shu, D, Yang, Q, et al. Local Stress/Strain Field Analysis of Die-Casting Al Alloys via 3D Model Simulation with Realistic Defect Distribution and RVE Modelling. Eng. Fail. Anal. 2025, 168, 109104.
- [159] Li, G, Li, B, Bai, X, Chen, H, et al. Research Advances in Multi-Scale Numerical Simulations of Forming and Microstructures for Magnesium Alloys. J. Magnes. Alloys 2024, 12 (10), 3898–3946.
- [160] Rapp, B E. Chapter 10 Conservation of Mass: The Continuity Equation. In *Microfluidics (Second Edition)*; Rapp, B. E., Ed.; Micro and Nano Technologies; Elsevier, 2023; pp 283–289.
- [161] Rapp, B E. Chapter 11 Conservation of Momentum: The Navier-Stokes Equation. In *Microfluidics (Second Edition)*; Rapp, B. E., Ed.; Micro and Nano Technologies; Elsevier, 2023; pp 291–309.
- [162] Ishikawa, S, Kijimoto, S. Modal Analysis for Incompressible Fluid Flow: Proposed Treatment of Inlet and Outlet Boundary Conditions. Eur. J. Mech. - BFluids 2025, 113, 204271.
- [163] Soh, W Y, Goodrich, J W. Unsteady Solution of Incompressible Navier-Stokes Equations. J. Comput. Phys. 1988, 79 (1), 113–134.
- [164] Harlow, F H, Welch, J E. Numerical Calculation of Time-Dependent Viscous Incompressible Flow of Fluid with Free Surface. Phys. Fluids 1965, 8 (12), 2182–2189.
- [165] Amsden, A A, Harlow, F H. A Simplified MAC Technique for Incompressible Fluid Flow Calculations. J. Comput. Phys. 1970, 6 (2), 322–325.
- [166] Chorin, A J. A Numerical Method for Solving Incompressible Viscous Flow Problems. J. Comput. Phys. 1967, 2 (1), 12–26.

- [167] NIYAMA, E, UCHIDA, T, MORIKAWA, M, SAITO, S. METHOD OF SHRINKAGE PREDICTION AND ITS APPLICATION TO STEELCASTING PRACTICE. AFS INT CAST MET J 1982, V 7 (N 3), 52–63.
- [168] Fu, P X, Kang, X H, Ma, Y C, Liu, K, et al. Centrifugal Casting of TiAl Exhaust Valves. Intermetallics 2008, 16 (2), 130–138.
- [169] Nastac, L. Modelling Approach for Quantitative Prediction of Macroshrinkage and Microshrinkage in A356 Sand Mould Castings. Int. J. Cast Met. Res. 2012, 25 (3), 144–154.
- [170] Li, J, Chen, R, Ma, Y, Ke, W. Characterization and Prediction of Microporosity Defect in Sand Cast WE54 Alloy Castings. J. Mater. Sci. Technol. 2014, 30 (10), 991–997.
- [171] Cao, H, Wang, C, Shan, Q, Che, J, et al. Kinetic Analysis of Pore Formation in Die-Cast Metals and Influence of Absolute Pressure on Porosity. Vacuum 2019, 168, 108828.
- [172] Wang, Z, Song, J, Huang, Y, Srinivasan, A, et al. An Investigation on Hot Tearing of Mg-4.5Zn-(0.5Zr) Alloys with Y Additions. Metall. Mater. Trans. A 2015, 46 (5), 2108–2118.
- [173] Jadhav, A R, Hujare, D P, Hujare, P P. Design and Optimization of Gating System, Modification of Cooling System Position and Flow Simulation for Cold Chamber High Pressure Die Casting Machine. Mater. Today Proc. 2021, 46, 7175–7181.
- [174] W, O. A Quantitative Approach to Casting Solidification Freezing of Cast Iron. Trans Am Soc Met 1966, No. 59, 945–961.
- [175] Hunt, J D, Lu, S-Z. Numerical Modelling of Cellular and Dendritic Array Growth: Spacing and Structure Predictions. Mater. Sci. Eng. A 1993, 173 (1), 79–83.
- [176] Thévoz, Ph, Desbiolles, J L, Rappaz, M. Modeling of Equiaxed Microstructure Formation in Casting. Metall. Trans. A 1989, 20 (2), 311–322.
- [177] Rappaz, M, Thévoz, PH. Solute Diffusion Model for Equiaxed Dendritic Growth. Acta Metall. 1987, 35 (7), 1487–1497.
- [178] Kurz, W, Giovanola, B, Trivedi, R. Theory of Microstructural Development during Rapid Solidification. Acta Metall. 1986, 34 (5), 823–830.
- [179] Spittle, J A, Brown, S G R. Computer Simulation of the Effects of Alloy Variables on the Grain Structures of Castings. Acta Metall. 1989, 37 (7), 1803–1810.
- [180] Spittle, J A, Brown, S G R. A Computer Simulation of the Influence of Processing Conditions on As-Cast Grain Structures. J. Mater. Sci. 1989, 24 (5), 1777–1781.

- [181] Natsume, Y, Ohsasa, K. Prediction of Casting Structure in Aluminum-Base Multi-Component Alloys Using Heterogeneous Nucleation Parameter. ISIJ Int. 2006, 46 (6), 896–902.
- [182] Gong, T Z, Chen, Y, Cao, Y F, Kang, X H, et al. Fast Simulations of a Large Number of Crystals Growth in Centimeter-Scale during Alloy Solidification via Nonlinearly Preconditioned Quantitative Phase-Field Formula. Comput. Mater. Sci. 2018, 147, 338–352.
- [183] Huo, L, Han, Z, Liu, B. Modeling and Simulation of Microstructure Evolution of Cast Mg Alloy. Mater. Sci. Forum 2010, 638–642, 1562–1568.
- [184] Böttger, B, Eiken, J, Ohno, M, Klaus, G, et al. Controlling Microstructure in Magnesium Alloys: A Combined Thermodynamic, Experimental and Simulation Approach. Adv. Eng. Mater. 2006, 8 (4), 241–247.
- [185] Wu, M, Hua, L, Xiong, S. Modeling Studies on Divorced Eutectic Formation of High Pressure Die Cast Magnesium Alloy. China Foundry 2018, 15 (1), 58–65.
- [186] Wang, X-Y, Wang, F-F, Wu, K-Y, Wang, X-F, et al. Experimental Study and Cellular Automatonsimulation on Solidification Microstructure of Mg-Gd-Y-Zr Alloy. Rare Met. 2021, 40 (1), 128-136.
- [187] Zhao, Y, Pu, Z, Wang, L, Liu, D-R. Modeling of Grain Refinement and Nucleation Behavior of Mg-4Y-0.5Zr (Wt.%) Alloy via Cellular Automaton Model. Int. J. Met. 2022, 16 (2), 945–961.
- [188] Wang, Y, Jia, S, Wei, M, Peng, L, et al. Coupling in Situ Synchrotron X-Ray Radiography and Phase-Field Simulation to Study the Effect of Low Cooling Rates on Dendrite Morphology during Directional Solidification in Mg–Gd Alloys. J. Alloys Compd. 2020, 815, 152385.
- [189] Li, Q, Guo, Q, Li, R. Modeling Solidification Structure Evolution and Microsegregation under Pressure Condition. J. Univ. Sci. Technol. Beijing Miner. Metall. Mater. 2006, 13 (6), 516–522.
- [190] Pan, H, Han, Z, Liu, B. Study on Dendritic Growth in Pressurized Solidification of Mg-Al Alloy Using Phase Field Simulation. J. Mater. Sci. Technol. 2016, 32 (1), 68-75.
- [191] Lin, L, Wang, F, Yang, L, Chen, L J, et al. Microstructure Investigation and First-Principle Analysis of Die-Cast AZ91 Alloy with Calcium Addition. Mater. Sci. Eng. A 2011, 528 (15), 5283–5288.
- [192] Yang, Q, Bu, F, Qiu, X, Li, Y, et al. Strengthening Effect of Nano-Scale Precipitates in a Die-Cast Mg-4Al-5.6Sm-0.3Mn Alloy. J. Alloys Compd. 2016, 665, 240-250.

- [193] Lv, S, Li, Y, Meng, F, Duan, Q, et al. Thermodynamic Stability of All1RE3 Intermetallic Compounds from First-Principles Calculations. Comput. Mater. Sci. 2017, 131, 28–34.
- [194] Yang, Q, Liu, X, Bu, F, Meng, F, et al. First-Principles Phase Stability and Elastic Properties of Al–La Binary System Intermetallic Compounds. Intermetallics 2015, 60, 92–97.
- [195] Xie, H, Huang, Q, Bai, J, Li, S, et al. Nonsymmetrical Segregation of Solutes in Periodic Misfit Dislocations Separated Tilt Grain Boundaries. Nano Lett. 2021, 21 (7), 2870–2875.
- [196] Kulekci, M K. Magnesium and Its Alloys Applications in Automotive Industry. Int. J. Adv. Manuf. Technol. 2008, 39 (9), 851–865.
- [197] Yang, Q, Guan, K, Qiu, X, Zhang, D, et al. Structures of Al2Sm Phase in a High-Pressure Die-Cast Mg-4Al-4Sm-0.3Mn Alloy. Mater. Sci. Eng. A 2016, 675, 396-402.
- [198] Zhu, S, Wong, C, Styles, M J, Abbott, T B, et al. Revisiting the Intermetallic Phases in High-Pressure Die-Cast Mg-4Al-4Ce and Mg-4Al-4La Alloys. Mater. Charact. 2019, 156, 109839.
- [199] Li, X, Xiong, S M, Guo, Z. Improved Mechanical Properties in Vacuum-Assist High-Pressure Die Casting of AZ91D Alloy. J. Mater. Process. Technol. 2016, 231, 1–7.
- [200] Le, T, Wei, Q, Wang, J, Jin, P, et al. Effect of Different Casting Techniques on the Microstructure and Mechanical Properties of AE44-2 Magnesium Alloy. Mater. Res. Express 2020, 7 (11), 116513.
- [201] Liu, X, Le, T, Yuan, S, Wang, J, et al. The Microstructure and Quasi-Static Compression Properties at Elevated Temperatures of the Aged Vacuum Die-Casting Mg-4Al-4(La, Ce) Alloy. J. Mater. Res. Technol. 2023, 23, 4293–4306.
- [202] Wang, Z, Zhang, B, Li, D, Fritzsch, R, et al. Effect of Heat Treatment on Microstructures and Mechanical Properties of High Vacuum Die Casting Mg-8Gd-3Y-0.4Zr Magnesium Alloy. Trans. Nonferrous Met. Soc. China 2014, 24 (12), 3762-3768.
- [203] Cong, W, Wang, F, Du, X, Wang, Z, et al. Study on Microstructure, Mechanical Properties and Thermal Conductivity of Vacuum-Assisted High Pressure Die Casting Mg-5Zn-xCu-0.5Zr Alloy. Mater. Sci. Eng. A 2025, 938, 148478.
- [204] Liu, H, Bae, J-H, Kang, J-W, Lee, J-S, et al. Effect of Cooling Rate on Corrosion Resistance and Behavior of Micro-Alloyed Cast AZ91-Ca-Y Alloy. J. Magnes.

Alloys 2025.

- [205] Özarslan, S, Şevik, H, Sorar, İ. Microstructure, Mechanical and Corrosion Properties of Novel Mg-Sn-Ce Alloys Produced by High Pressure Die Casting. Mater. Sci. Eng. C 2019, 105, 110064.
- [206] Xiao, B, Song, G-L, Zheng, D, Cao, F. A Corrosion Resistant Die-Cast Mg-9Al-1Zn Anode with Superior
- Discharge Performance for Mg-Air Battery. Mater. Des. 2020, 194, 108931.
- [207] Wen, W, Luo, A A, Zhai, T, Jin, Y, et al. Improved Bending Fatigue and Corrosion Properties of a Mg-Al-Mn Alloy by Super Vacuum Die Casting. Scr. Mater. 2012, 67 (11), 879–882